SITING WIND TURBINES TO MINIMIZE RAPTOR COLLISIONS AT SAND HILL REPOWERING PROJECT, ALTAMONT PASS WIND RESOURCE AREA

K. Shawn Smallwood and Lee Neher

15 March 2016

EXECUTIVE SUMMARY

Map-based collision hazard models were prepared as a set of tools to help guide the careful siting of proposed new wind turbines as part of the repowering effort at Sand Hill in the Alameda County portion of the Altamont Pass Wind Resource Area (APWRA). Similar collision hazard models were prepared for the Tres Vaqueros and Vasco Winds repowering projects in Contra Costa County and for the Patterson Pass, Golden Hills and Golden Hills North repowering projects in Alameda County. After three years of fatality monitoring following construction, it was found that the repowering of Vasco Winds reduced fatalities of raptors and of all birds as a group. This newest set of models for Sand Hill benefit from the lessons learned at Vasco Winds, as well as from many additional data collected through 2015 and the emergence of dependent variables and predictor variables that we believe result in superior collision hazard models.

Our collision hazard model for golden eagle (*Aquila chrysaetos*) was derived from 121,259 GPS/GSM telemetry positions within the APWRA, as well as from thousands of behavior records made during visual scans and from fatality rates at wind turbines monitored from 1998 through 2011. Our collision hazard model for red-tailed hawk (*Buteo jamaicensis*) was derived from thousands of behavior records and from estimates of fatality rates at wind turbines, and our American kestrel (*Falco sparverius*) model was derived from thousands of behavior observations throughout the APWRA. Our collision hazard model for burrowing owl (*Athene cunicularia*) was derived from 5 years of burrowing owl surveys in 46 plots located throughout the APWRA, as well as from estimates of fatality rates at wind turbines.

Based on our models, we predict greatly reduced fatality rates of red-tailed hawks, American kestrels, burrowing owls and all birds as a group. Golden eagles were rarely killed by wind turbines at Sand Hill, with only 3 documented fatalities since 1998, even though Sand Hill was the most intensively monitored wind project in the APWRA. Given the airspace that will be opened up to safe golden eagle traffic, we believe the golden eagle fatality rate will lessen from its already low level. American kestrel fatalities will likely lessen due to the elimination of the many small wind turbines that not only caused collision fatalities but also entrapped kestrels in hollow tubes of the lattice towers and within the turbine machinery. Burrowing owl fatalities have been very high at Sand Hill relative to most of the rest of the APWRA, but the repowering project should reduce burrowing owl fatalities by 90% or better. Further contributing to fatality reductions, Ogin was able to accommodate 5 of our 6 recommended turbine relocations to minimize collision risk to golden eagles and red-tailed hawks. Based on our experience at Vasco Winds, the fatality rates of bats might increase from the old projects at Sand Hill, but most of the fatality monitoring performed at Sand Hill was inadequate for detecting bat fatalities so it will be difficult to determine the repowering projects effects on bats.

INTRODUCTION

Ogin, Inc. plans to install 12 3-MW turbines as part of its Sand Hill repowering project in the Alameda County portion of the Altamont Pass Wind Resource Area ("APWRA"), California. Careful siting of wind turbines is one of the principal measures available to minimize raptor fatalities caused by collisions with the turbines (Smallwood and Thelander 2004, Smallwood and Karas 2009, Smallwood and Neher 2009). The objective of this approach is to carefully site new wind turbines to minimize the frequencies at which raptors of various species encounter the wind turbines while flying, but most especially while performing specific types of flight behaviors, such as low flights crossing ridge-like topographic features in the case of golden eagles and hovering or kiting in the cases of red-tailed hawks and American kestrels. In this study we developed simple Fuzzy Logic (FL) models (Tanaka 1997) of raptor activity quantified from behavior data collected across the APWRA between 13 November 2012 and 29 October 2015, and at special studies performed at Sand Hill sites between 30 April 2012 and 5 March 2015 and Patterson Pass between 15 October 2013 and 24 September 2014. The behaviors used in the modeling effort were derived from the results of Smallwood et al. (2009b), and an example application of the FL modeling approach can be seen in Smallwood et al. (2009a).

The Fuzzy Logic approach is a rule-based system useful with noisy data or with zero-dominated data sets, and is applied to events occurring within classes that are assumed to have graduated rather than sharp boundaries (Tanaka 1997). The rules consist of assigning likelihood values of an event occurring, which in the case of this study would be the likelihood of a bird performing a specific behavior within a cell of an analytical grid laid over the project area. Likelihood values can range 0 to 1 for each predictor variable, depending on how far a value of the predictor variable differs from the mean where the event has been recorded. The magnitude of each deviation from the mean is assessed by the analyst based on error levels, data distribution, and the analyst's knowledge of the system. In our case, the events were of birds flying over terrain characterized by suites of slope conditions.

The study goal was to accurately predict the locations where golden eagles, red-tailed hawks, American kestrels and burrowing owls are most likely to perform flight behaviors putting these species at greater risk of collision with wind turbines, so that new wind turbines can be sited to avoid these locations. Achieving this goal depended on our understanding of how these species use terrain and wind, and how they perceive and react to wind turbines. It also depended on understanding patterns of fatality rates in the APWRA, so we also developed fatality rate models for golden eagle, red-tailed hawk, and burrowing owl (no model was predictive for American kestrel). Our model results were interpreted in tandem with Smallwood's familiarity with conditions associated with proposed wind turbine locations. By carefully siting the wind turbines to minimize collision risk, the Sand Hill project should prove safer to golden eagle, red-tailed hawk, and burrowing owl than the wind turbines being replaced. The Sand Hill micro-siting also benefits from what was learned at the Vasco Winds repowering project, which was micro-sited using a similar approach and monitored for collision fatalities for three years (Brown et al. 2013, 2014, 2015).

METHODS

On-site Assessments

One of us (Smallwood) typically visits the proposed repowering project site to assess the collision hazard associated with proposed wind turbine sites. In this case, however, we made no such visit because Smallwood was already very familiar with the sites, having overseen the monitoring of the old wind turbines for three years and having mapped fossorial mammal burrows and burrowing owl burrows across the properties involved.

Predictive Models

Multiple types of data were needed to develop collision hazard models. For developing collision hazard models of golden eagle, red-tailed hawk, and American kestrel, flight behavior data were collected and then related to terrain. For golden eagles, we also made use of GPS/GSM telemetry data collected from 18 golden eagles fitted with transmitters and flying over portions of the Altamont Pass Wind Resource Area. For burrowing owls, we recorded burrow locations and later related them to terrain. For all four raptor species, we estimated fatality rates among individual wind turbines monitored throughout the APWRA and over various time periods since 1998. And of course the terrain needed to be measured, and this was done using imagery, digital elevation models, and geoprocessing steps to bring objectivity to decisions about where a slope transitions from trending towards concavity to trending towards convexity, as an example. All of these data and the steps used to integrate them are covered in the following paragraphs. We begin with the biological survey data before describing the development of our digital elevation model (DEM) and terrain measurements, but we present the methods used for processing the GPS/GSM telemetry data until after the section on terrain measurements because we relied on our terrain measurements to screen the telemetry data for inclusion in the analysis.

Behavior data

Culminating 14 years of behavior surveys and utilization surveys in the APWRA (Smallwood et al. 2004, 2005, 2009b,c; Smallwood 2013), a new methodology was developed for behavior monitoring to benefit the development of wind turbine collision hazard models. The earlier behavior surveys recorded avian behaviors that were unmapped (Smallwood and Thelander 2004, 2005; Smallwood et al. 2009b), so no spatial analysis was possible. The mapping of bird locations emerged in 2002, but the 2002 approach was integrated with utilization surveys that were focused primarily on counting birds to estimate relative abundance. This mixing of objectives impinged on both objectives – on both the counting of birds and the mapping of their behavior patterns. On-the-minute mapping of bird locations and behaviors yielded only crude spatial patterns for only a few site-repetitive behaviors such as perching, kiting and hovering. After comparing use rates to fatality rates and seeing no significant spatial or inter-annual relationships between the two rates, it was decided to focus more on the behavior patterns to predict collision hazards. New methods were formulated to map flight behaviors.

Sixteen behavior observation stations were established among the Sand Hill sites (Figures 1 and 2), each location optimized to observe how golden eagles and other raptors behave in the

airspace around Ogin's BACI experimental treatment plots. The data from these stations were supplemented with data gathered from 9 stations in Patterson Pass and 36 stations across the rest of the APWRA (Figure 2). Twenty-one of these stations across the APWRA were selected from those that had been ranked from 1st through 30th in order of the number of first observations per hour per km^3 of visible airspace out to the maximum survey radius at each station during use surveys performed by the Alameda County Avian Monitor from 2005 through 2009. Fifteen additional stations were added to Vasco Caves Regional Preserve, Northern Territories, Vasco Winds Energy Project, and the Buena Vista Wind Energy Project in Contra Costa County, where the Alameda County Avian Monitor did very little work.

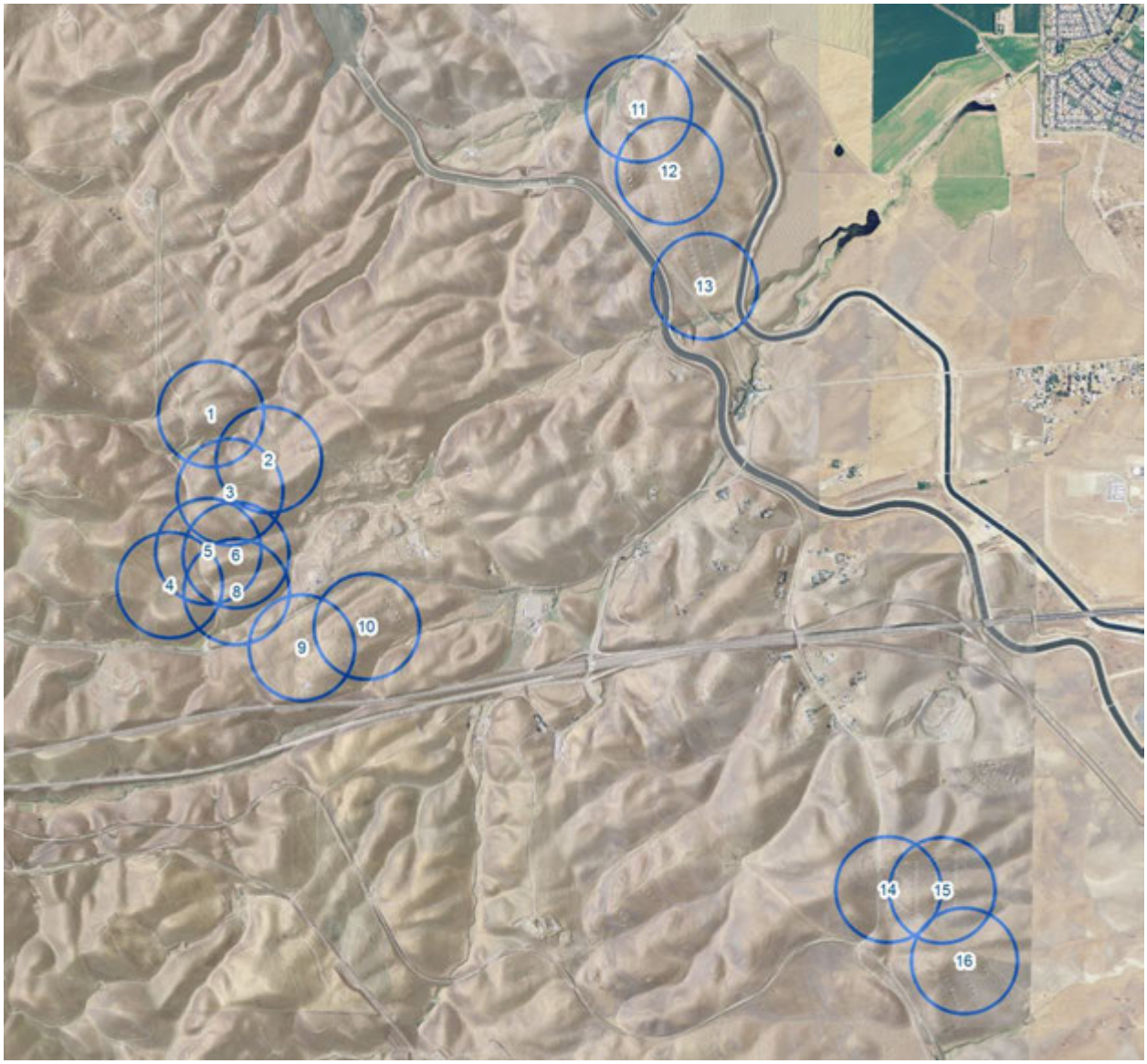

Figure 1. *Behavior survey plots within the Sand Hill project areas*.

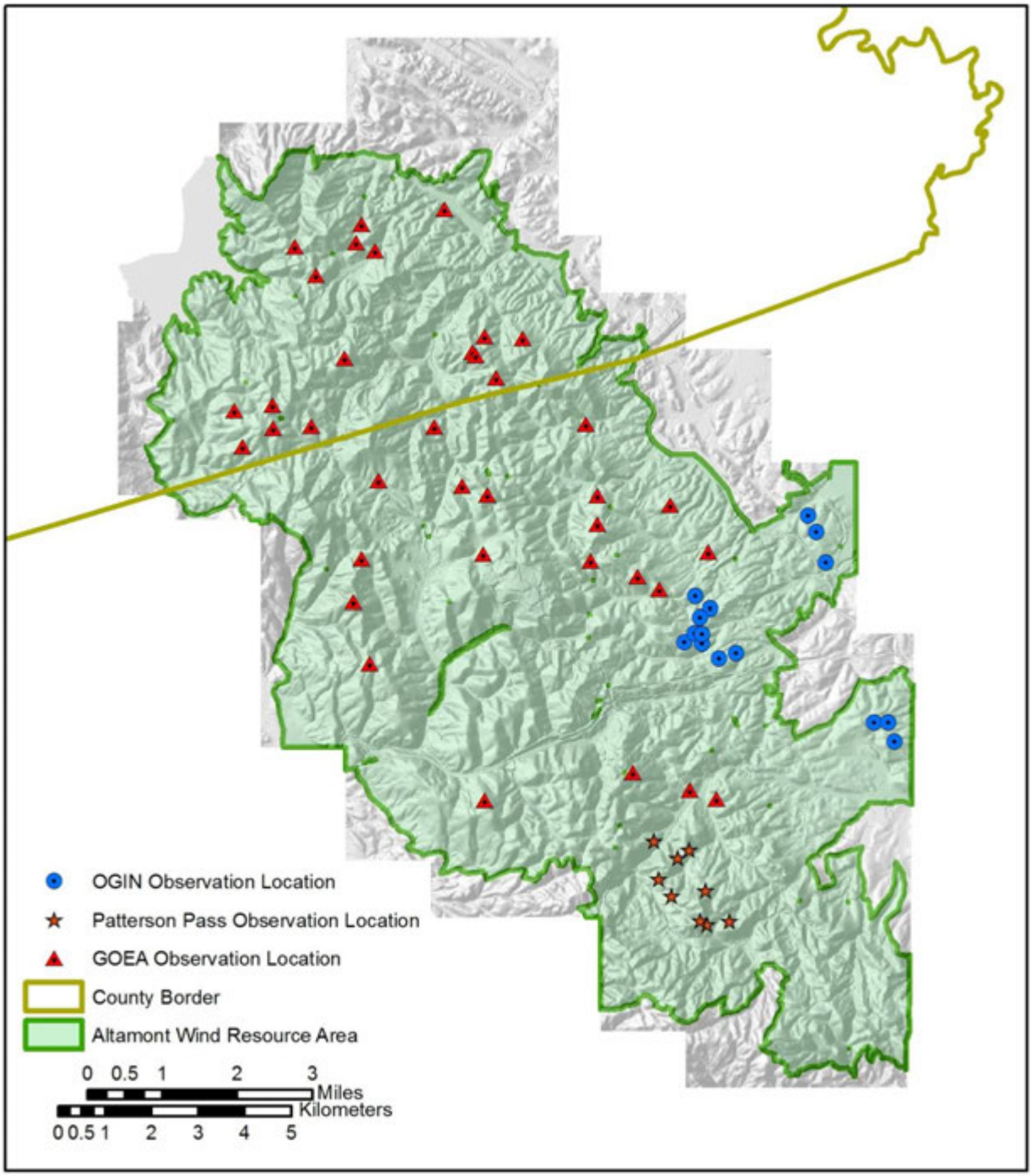

Figure 2. *Locations of behavior observation stations used for 30 min and 60 min visual scans to track individual birds and record behaviors and flight heights along the way*.

Behavior sessions at Sand Hill lasted 30 minutes each and elsewhere they lasted 1 hour each. Between 30 April 2012 and 5 March 2015 there were 2,002 surveys completed for 1,001 hours (126,084 birds tracked). The maximum survey radius depended on the printed map image extent and how far the observer felt comfortable estimating the bird's spatial location and height above ground. Map extents rarely permitted survey distances of >300 m. One of us (Smallwood)

recorded all of the behavior data within Patterson Pass, and additional behavior data were collected across the APWRA by Smallwood, Erika Walther, Brian Karas, and Harvey Wilson.

The 9 Patterson Pass stations were surveyed 167 times (167 hours) from 15 October 2013 to 24 September 2014 (5,712 birds tracked). The 36 APWRA stations were surveyed 928 times (928 hours) from 13 November 2012 through 29 October 2015 (27,552 birds tracked). Between all three studies, 2,096 hours of behavior surveys (159,348 birds tracked) provided the data used for developing collision hazard models reported herein.

Each bird was recorded onto image-based maps of the survey area as point features connected by vector lines depicting the bird's flight path (Figures 3-9). Height above ground, behavior, and time into the session was recorded into Tascam digital voice recorders fitted with windjammers designed to reduce noise buffeting by high winds. Point features were recorded as often as the observer could record attribute data into the voice recorder. One objective of the behavior sessions was to obtain high quality flight paths and summaries of flight behaviors of individual birds using the surveyed airspace, and it was notably not to count birds, although it was likely that just as many raptors were recorded as would have been counted based on the use survey protocols.

Another objective of the behavior surveys was to learn how birds interact with wind turbines when they approached the wind turbines. Special attention was given to the bird's flight whenever it flew within 50 m of a wind turbine and, in the opinion of the observer, faced the possibility of colliding with the wind turbine. During this time, the bird's approach angle to the turbine was recorded, as well as any changes in flight direction, flight height, behavior, interactions with other birds, and the wind turbine's operating status. Whenever special attention was directed to such flights, the flight observation was termed an "event," or a wind turbine interaction event.

At the start of each behavior session, the observer identified which wind turbines in the survey area were operating, as well as temperature, wind direction, average and maximum wind speed, and percentage cloud cover. Behavior data were transcribed to electronic spreadsheets within 24 hours of collection. Mapped bird location points and line features representing the bird's flight path were then digitized into the GIS.

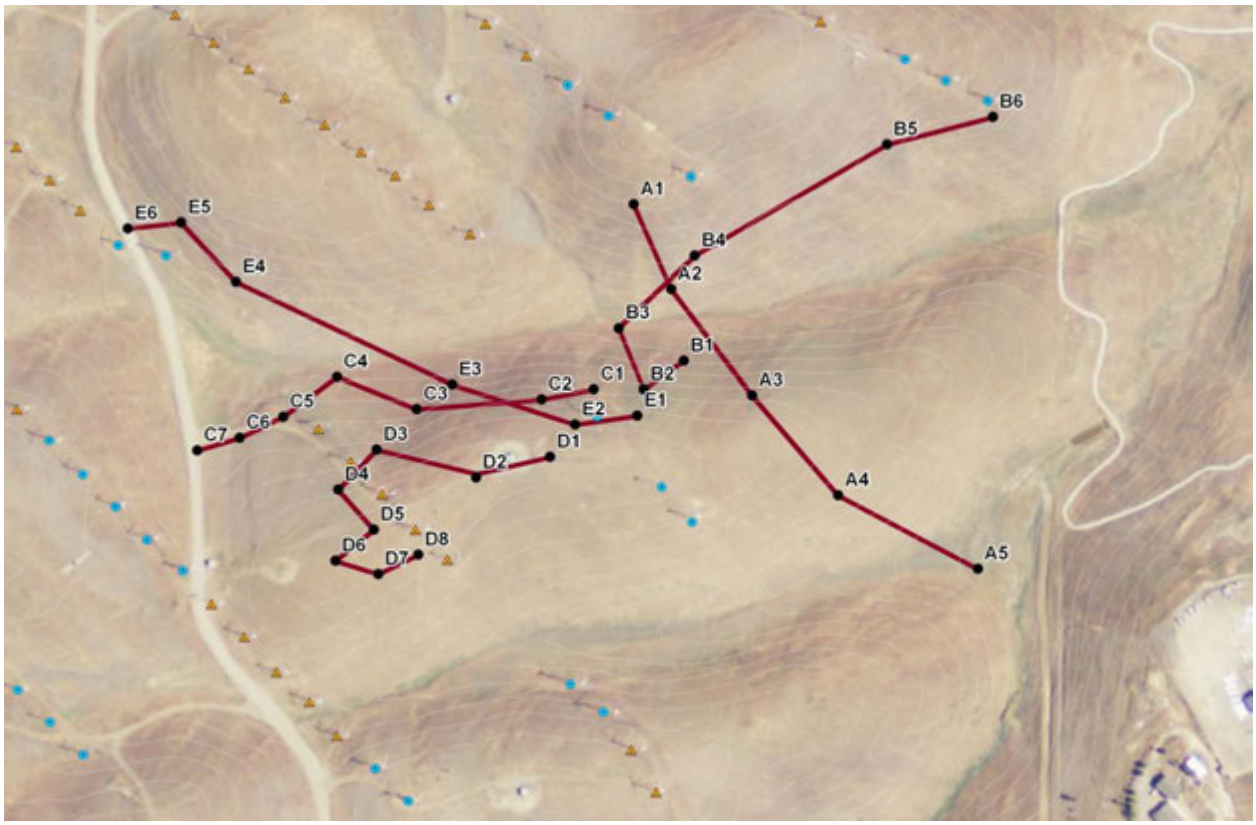

Figure 3. *Example of how birds were tracked visually during behavior surveys. Flight attributes were recorded at points, which were later connected by line segments representing a flight path. In this case 5 flight paths were recorded, A through E, and at each number associated with a point we also recorded behavior, height above ground, social group size and, when appropriate, wind turbine events. For example, D4 would likely have involved a wind turbine event*.

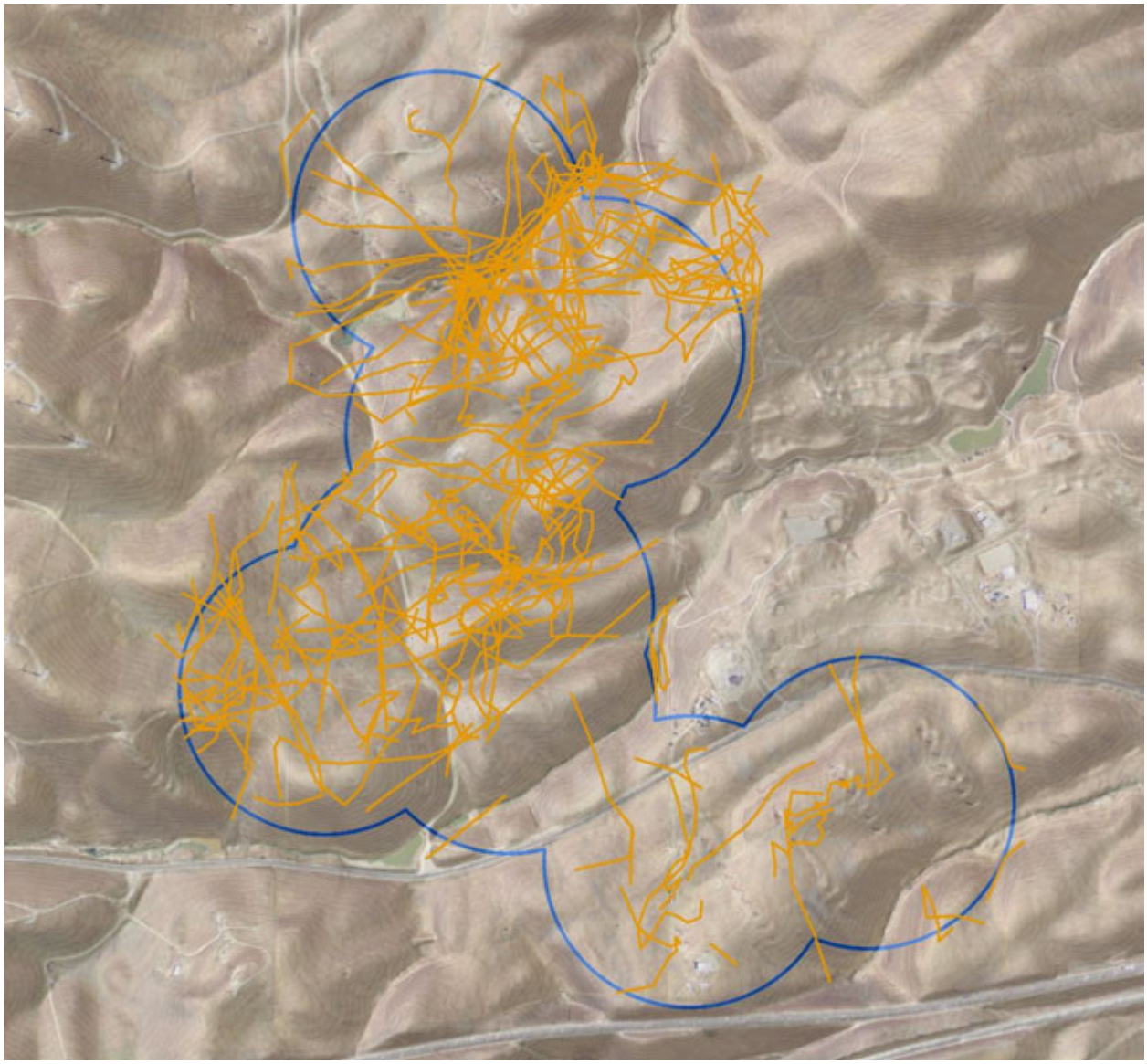

Figure 4. *Golden eagle flight paths recorded during 3 years of visual scans for behavior patterns within the vicinity of proposed turbines 1R through 5R, 2012-2015*.

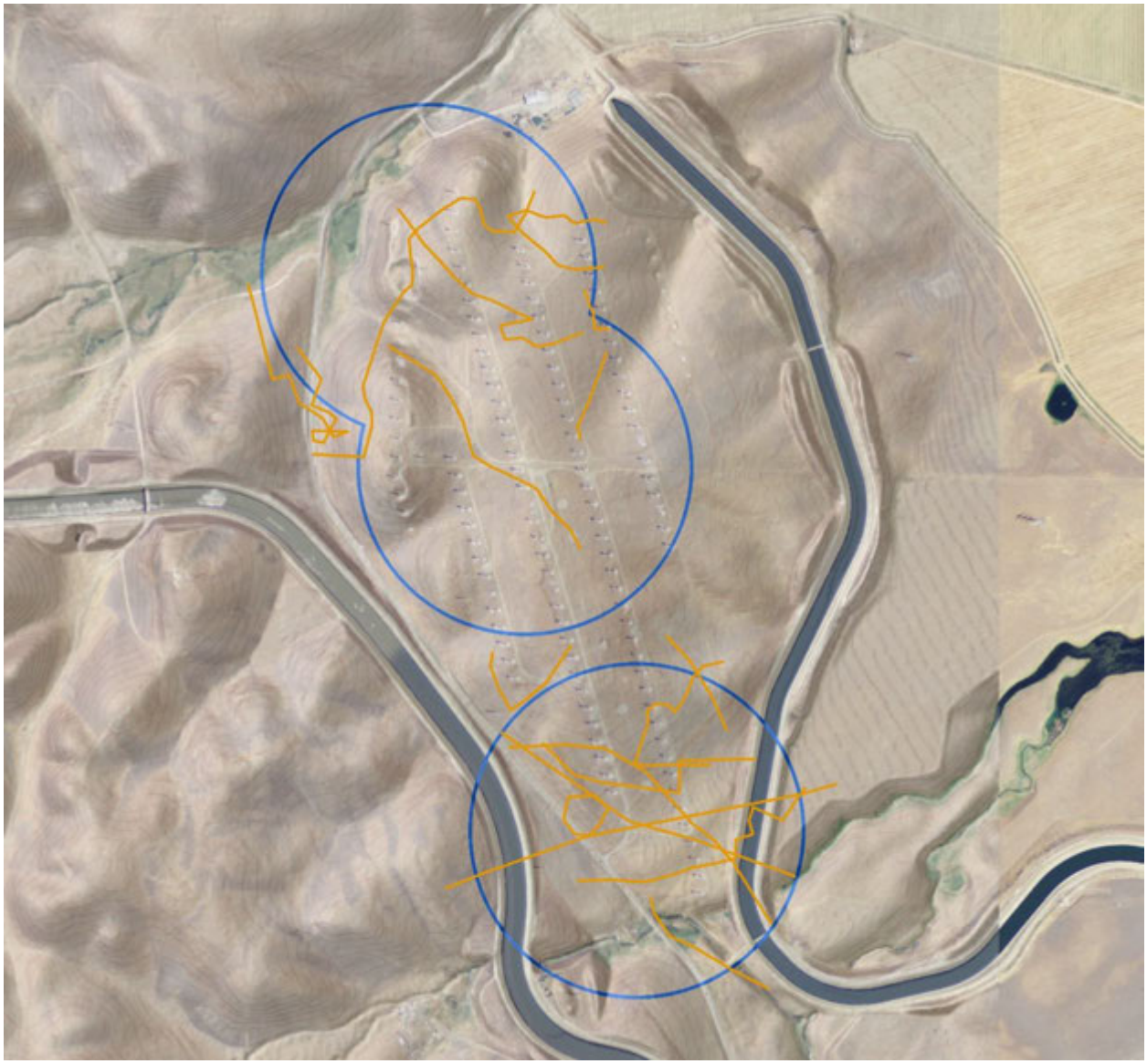

Figure 5. *Golden eagle flight paths recorded during 3 years of visual scans for behavior patterns within the vicinity of proposed turbines 6R through 9R, 2012-2015.*

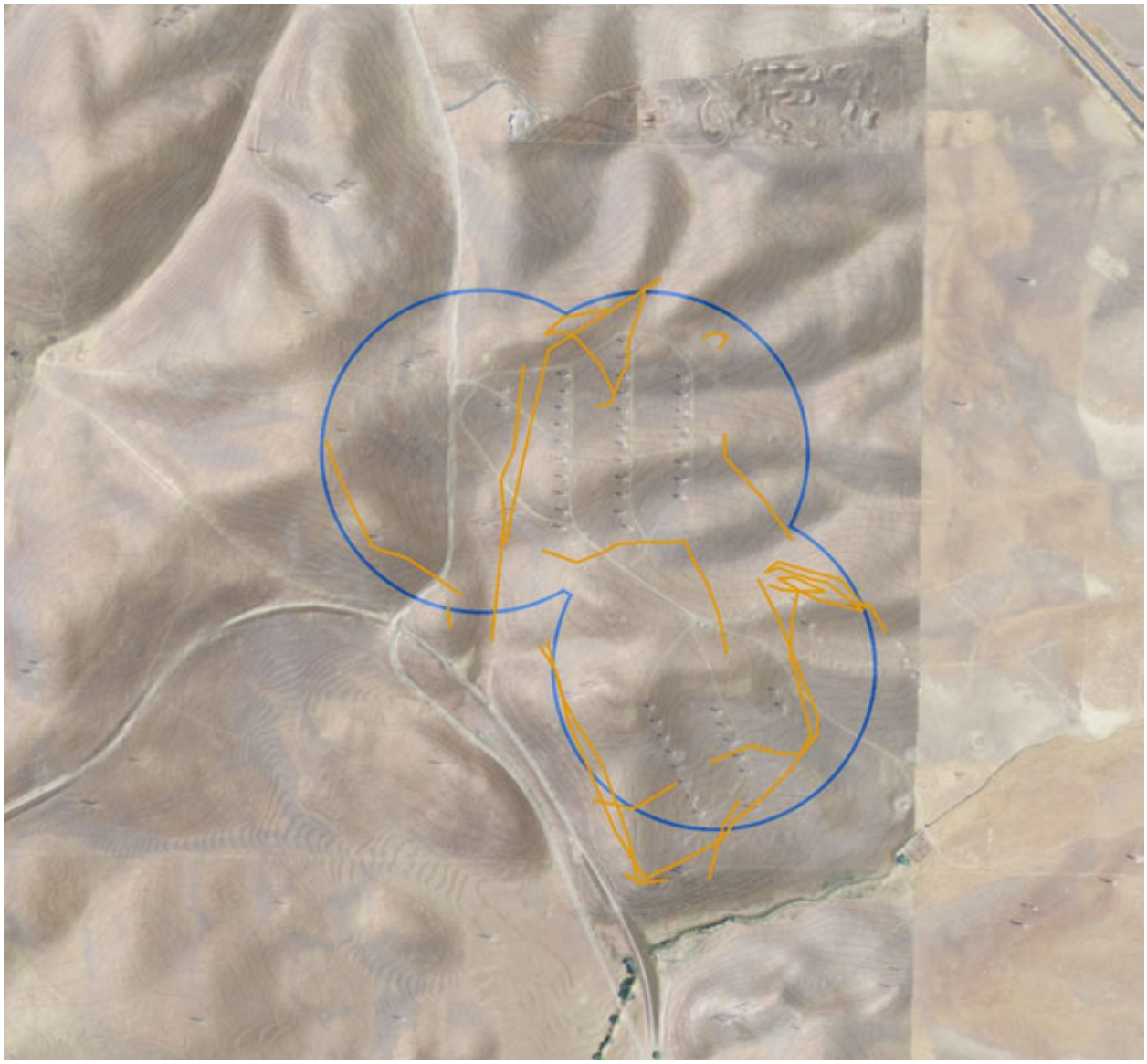

Figure 6. *Golden eagle flight paths recorded during 3 years of visual scans for behavior patterns within the vicinity of proposed turbines 10R through 12R, 2012-2015.*

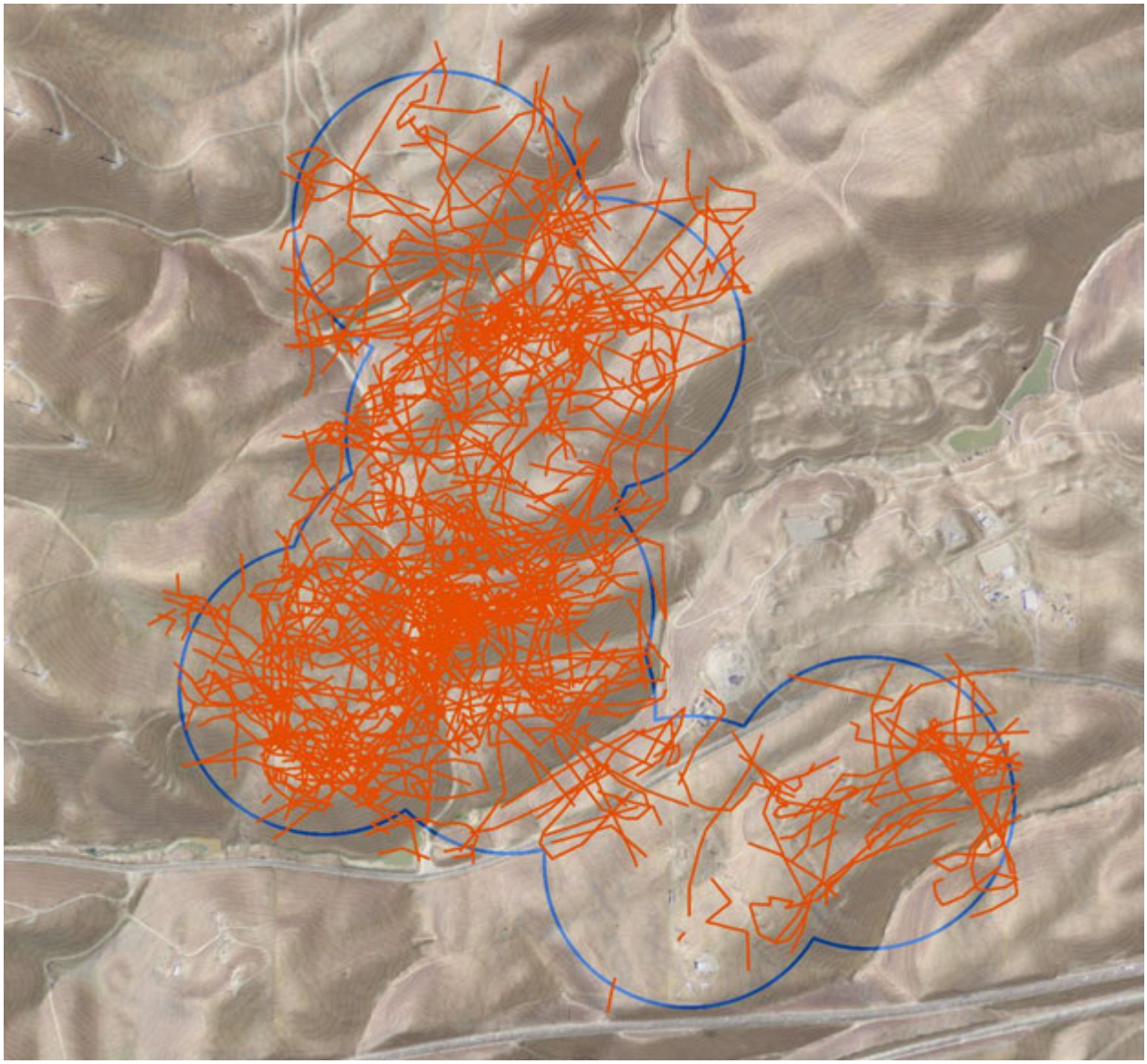

Figure 7. *Red-tailed hawk flight paths recorded during 3 years of visual scans for behavior patterns within the vicinity of proposed turbines 1R through 5R, 2012-2015.*

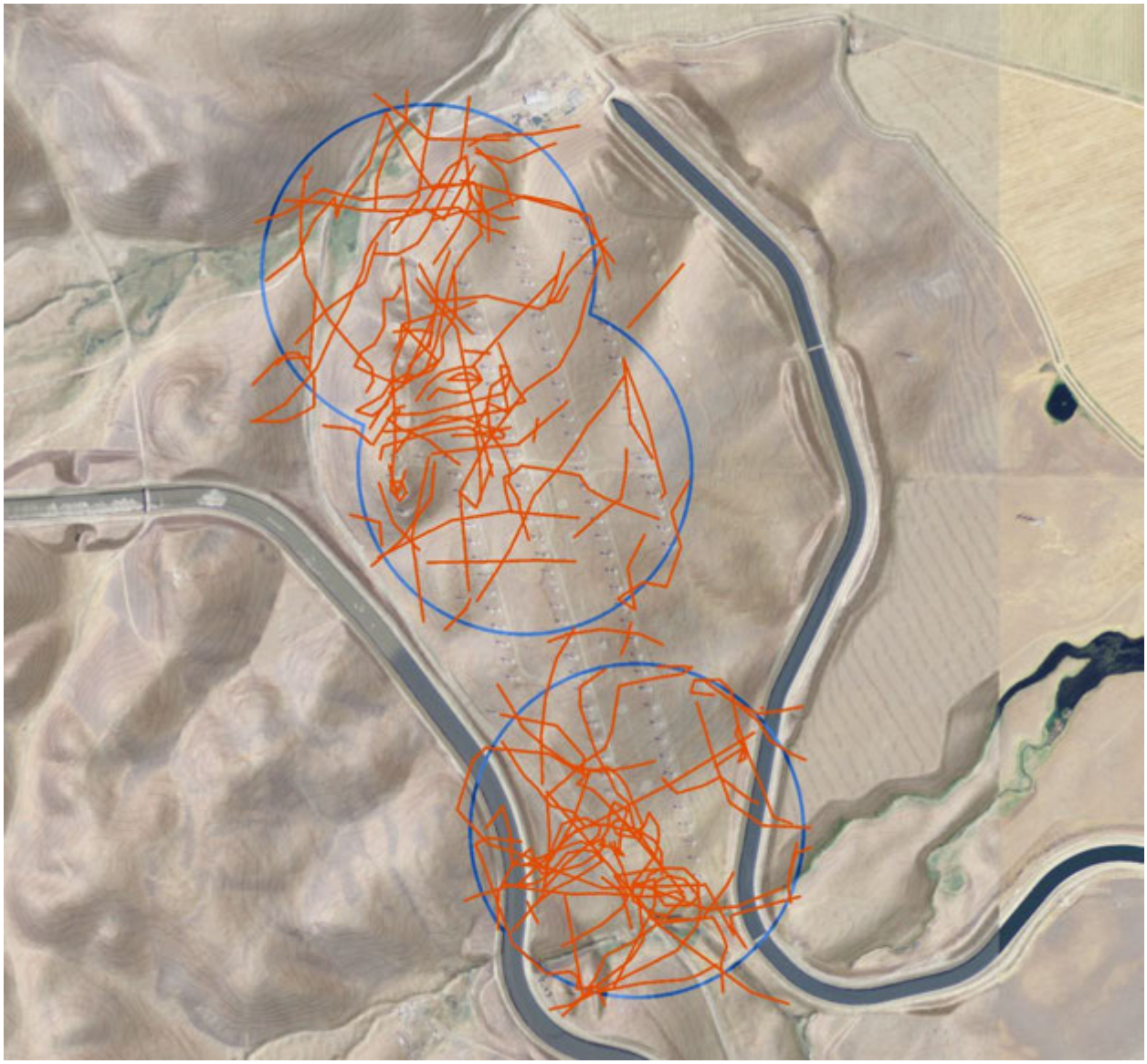

Figure 8. *Red-tailed hawk flight paths recorded during 3 years of visual scans for behavior patterns within the vicinity of proposed turbines 6R through 9R, 2012-2015.*

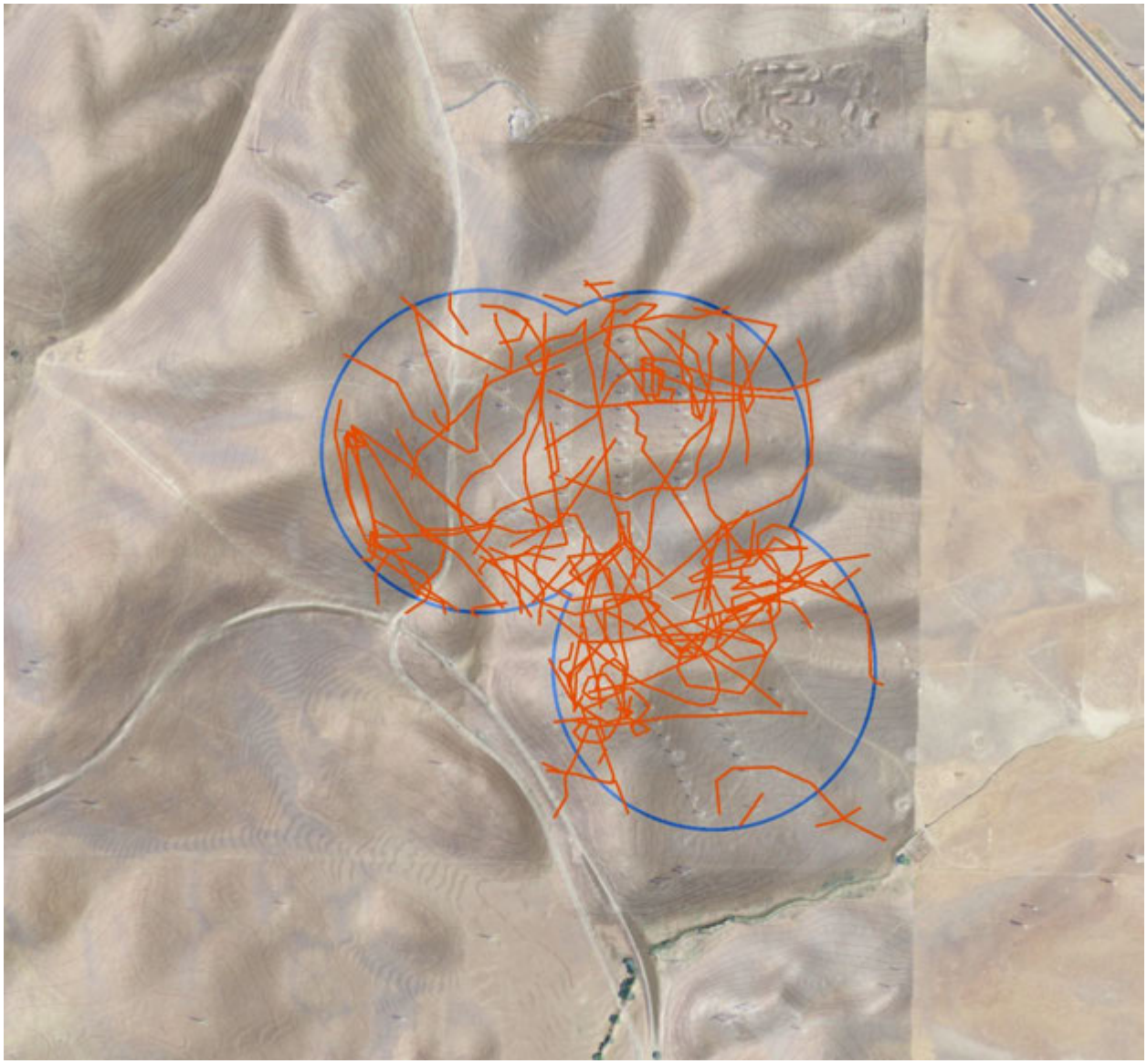

Figure 9. *Red-tailed hawk flight paths recorded during 3 years of visual scans for behavior patterns within the vicinity of proposed turbines 10R through 12R, 2012-2015.*

Figure 10. *American kestrel flight paths recorded during 3 years of visual scans for behavior patterns within the vicinity of proposed turbines 1R through 5R, 2012-2015.*

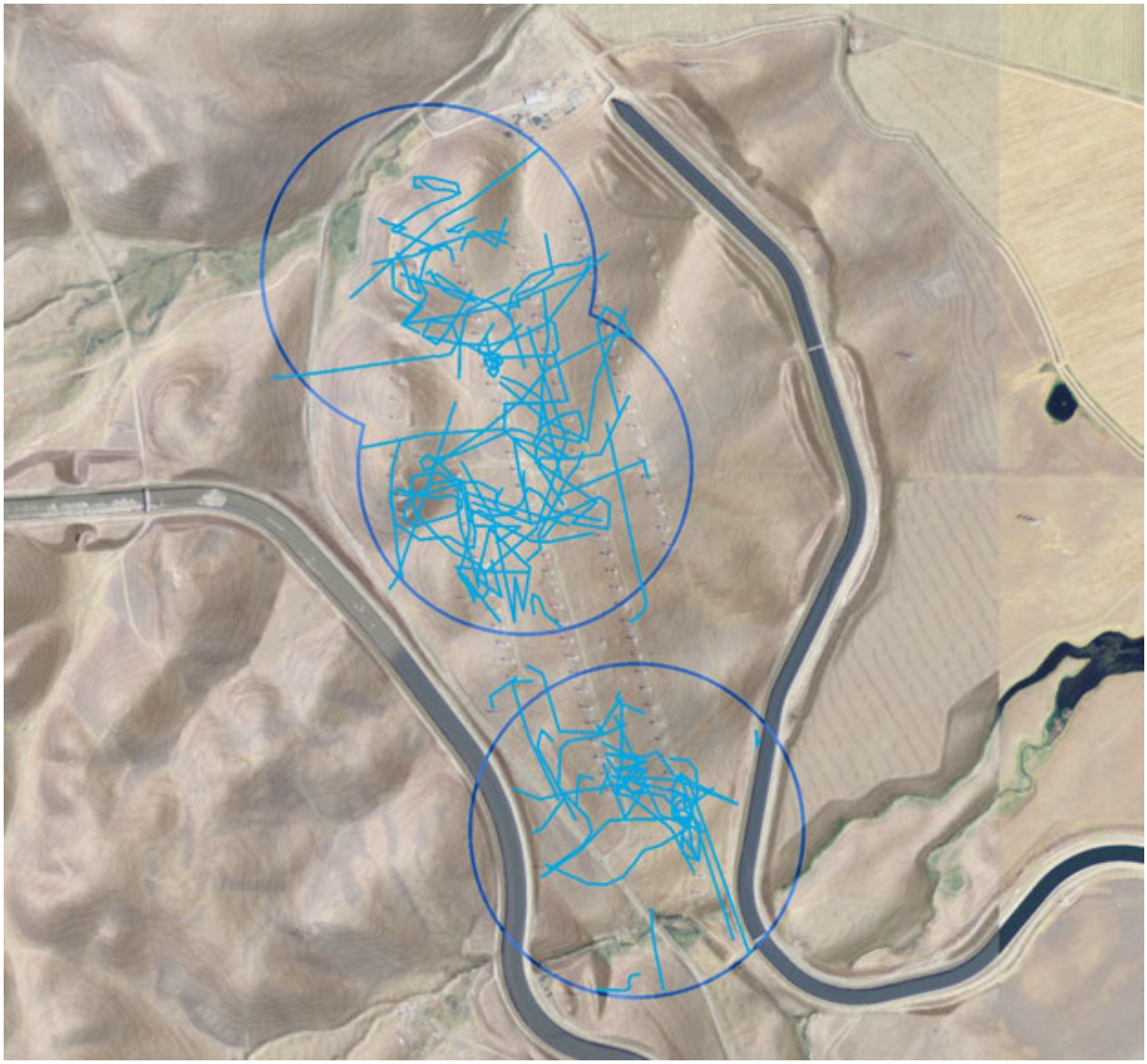

Figure 11. *American kestrel flight paths recorded during 3 years of visual scans for behavior patterns within the vicinity of proposed turbines 6R through 9R, 2012-2015.*

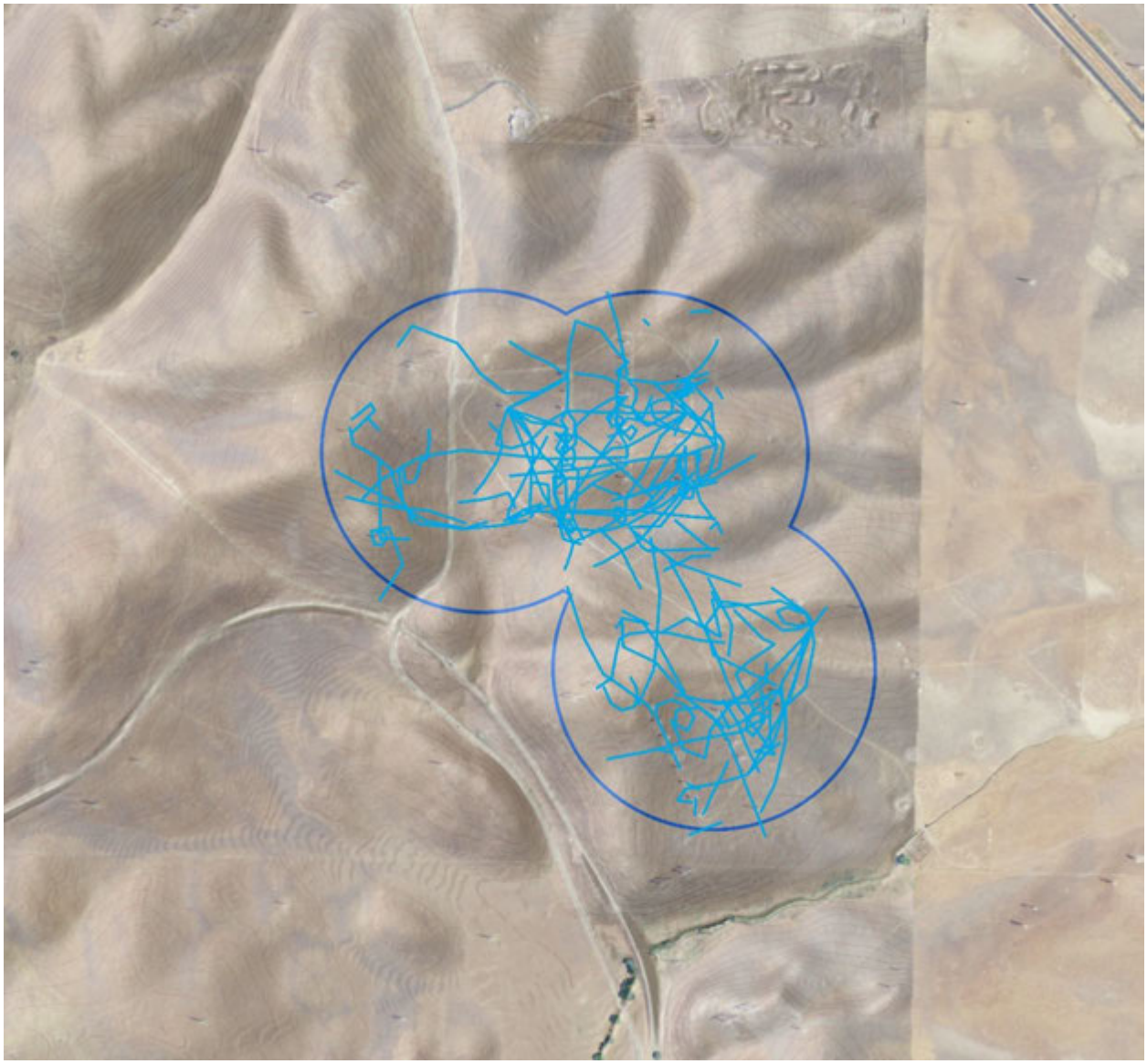

Figure 12. *American kestrel flight paths recorded during 3 years of visual scans for behavior patterns within the vicinity of proposed turbines 10R through 12R, 2012-2015.*

Burrowing owl burrows

Burrowing owl burrows (Figure 13)were mapped in sampling plots throughout the APWRA using a Trimble GeoXT GPS, both during the nesting season (Smallwood et al. 2013b) and throughout the year in 2011 (Figure 14). Additional burrow mapping efforts were made in follow-up visits during breeding seasons of 2012-2015. Most of the burrows that were mapped were nest burrows, but refuge burrows were also included in the data pool. No satellite burrows (alternate nest burrows) were used in the analysis.

Figure 13. *Example of a burrowing owl nest burrow, including an adult (foreground) and 3 chicks*.

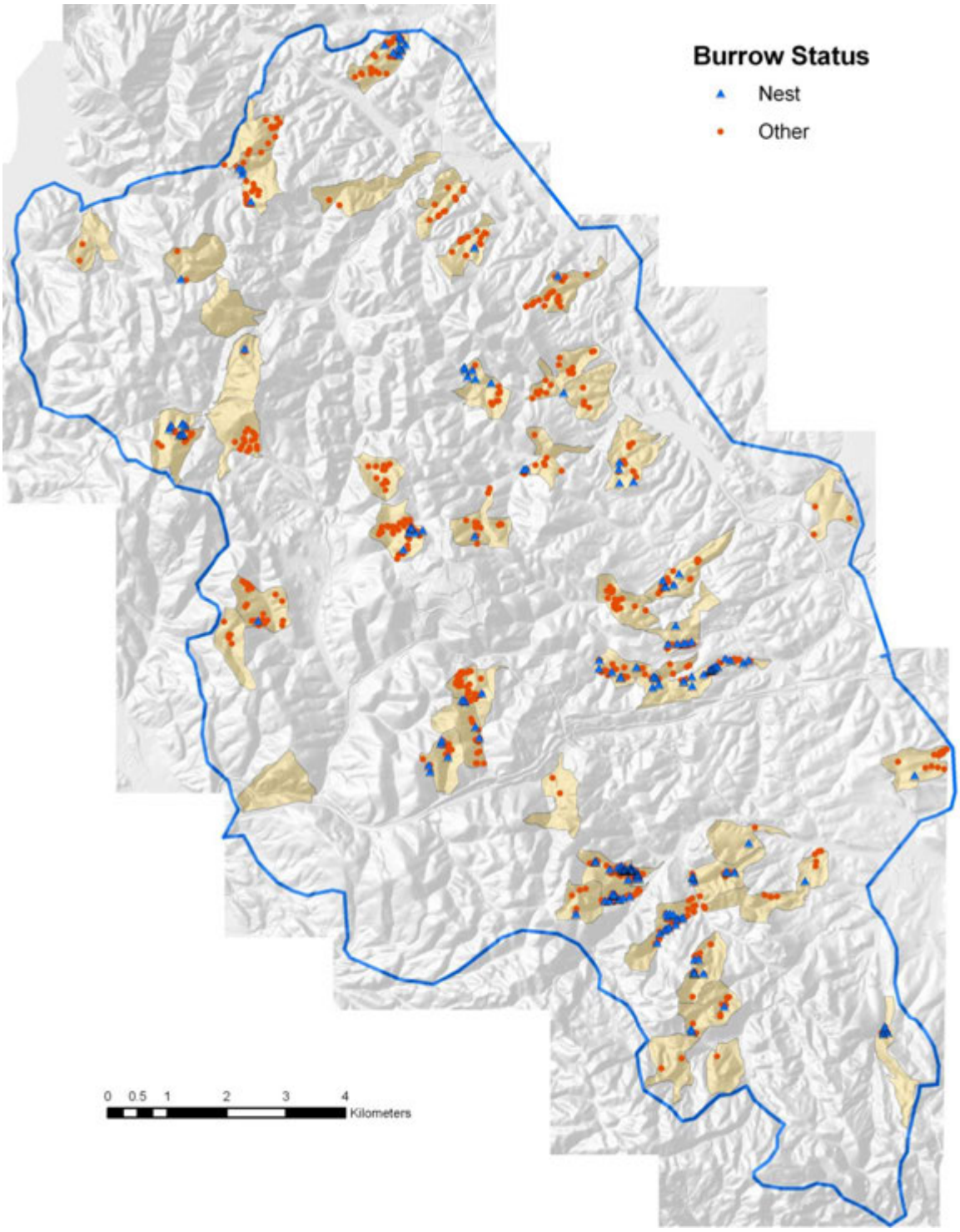

Figure 14. *Burrowing owl sampling plots (tan color) and 2011 nest and refuge burrow locations (as examples) within the Altamont Pass Wind Resource Area (blue polygon).*

Fatality rates

We estimated annual fatality rates at all old generation wind turbines that were searched at least one year between the years 1998 through 2011 in the APWRA. All fatality rates were adjusted for search detection and carcass persistence rates that were averaged among wind projects where trials were performed in similar grassland environments as compared to the APWRA (see Smallwood 2013). Fatality rates were also adjusted for variation in the maximum search radius, based on the method used by Smallwood (2013). Finally, we adjusted fatality rates for monitoring duration to account for the bias warned about in Smallwood and Thelander (2004:App. A); that is, as the number of fatalities is averaged into more years of survey effort, the resulting ratio of fatalities to years will decrease inversely with increasing number of years (Figure 15). This bias, which reflects a relatively constant number of fatalities (numerator) relative to a continuously varying number of years (denominator), was corrected by fitting an inverse function to the data, and then multiplying the ratio of observed to predicted values by the predicted value at 10 years of monitoring (Figure 15). In other words, all fatality rates at individual wind turbines were adjusted to a common 10-year period of monitoring, even if they had been monitored only one year, 4 years, or 10 years, etc. We also note that the fatality rate metric in this case excluded the turbine's rated capacity, MW.

Fatality rates adjusted for duration of monitoring were related to terrain measurements and terrain features to identify associations useful for developing predictive collision hazard models. The terrain features and terrain measurements used were those associated with the wind turbines where fatality rates had been recorded (Figure 16).

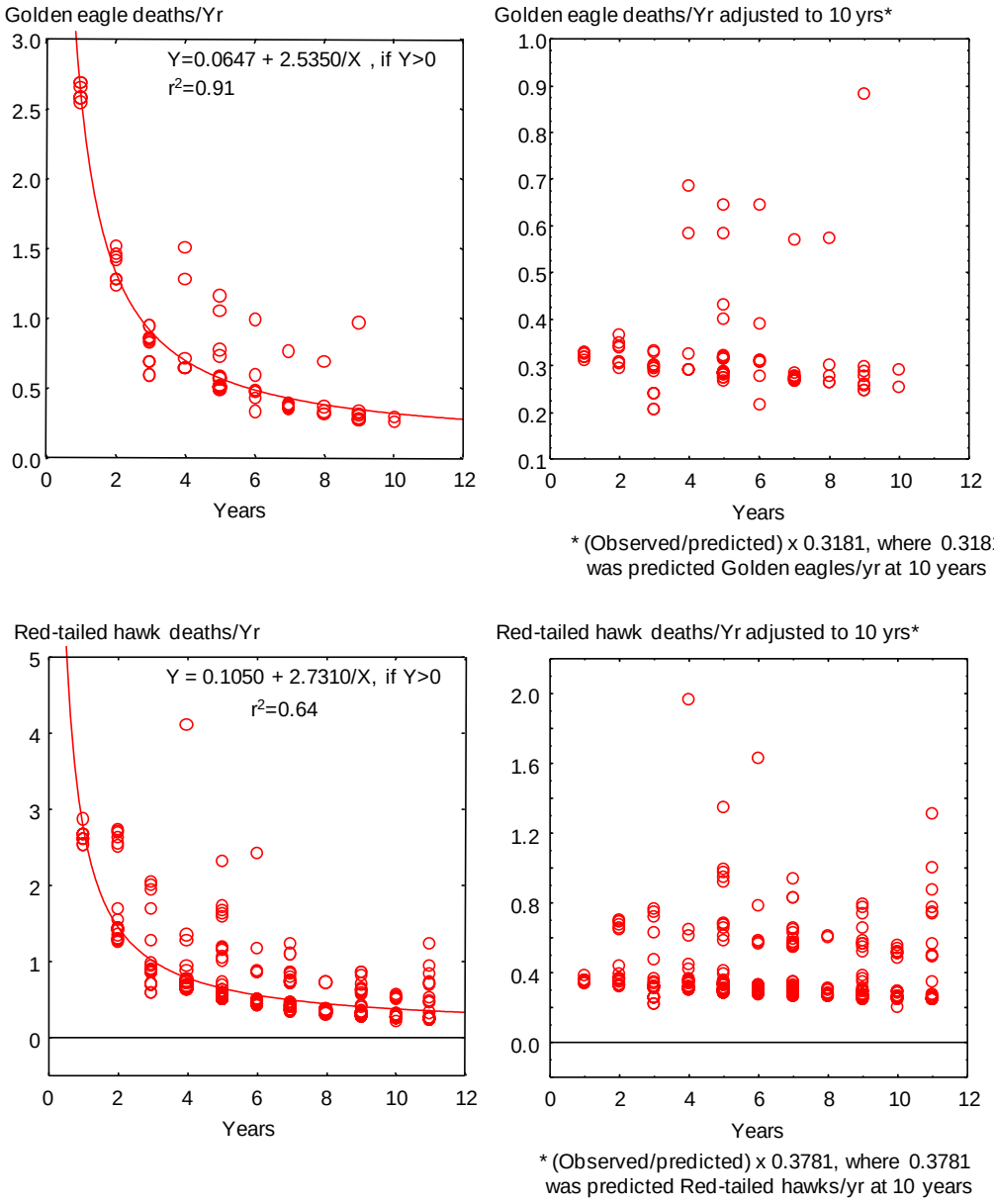

Figure 15a. *Mean annual fatalities/year declined inversely with the number of years used in the denominator for golden eagle and red-tailed hawk (left graphs), so fitting inverse functions to the data removed the effect of number of years on the metric (right graphs).*

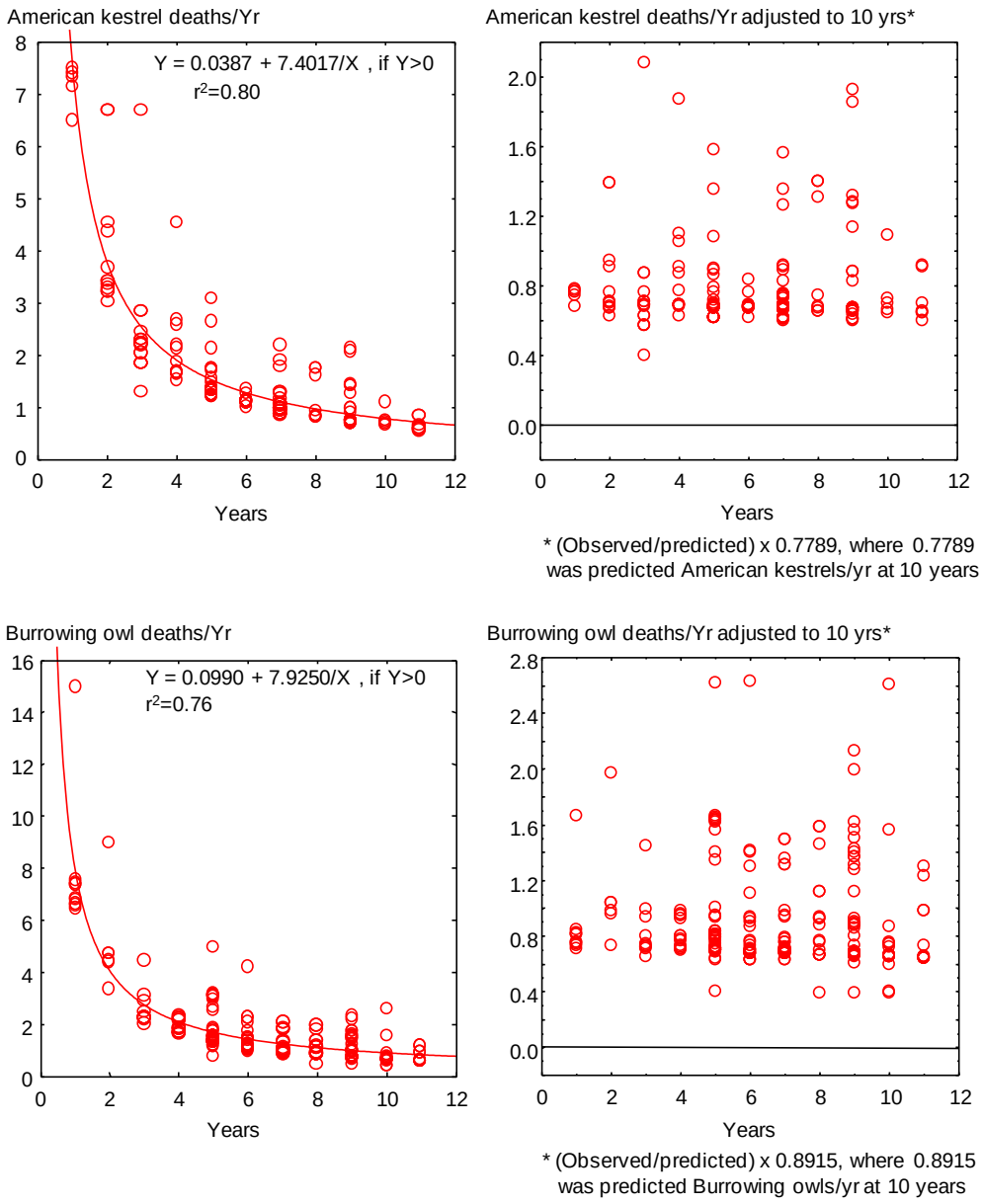

Figure 15b. *Mean annual fatalities/year declined inversely with the number of years used in the denominator for American kestrel and burrowing owl (left graphs), so fitting inverse functions to the data removed the effect of number of years on the metric (right graphs).*

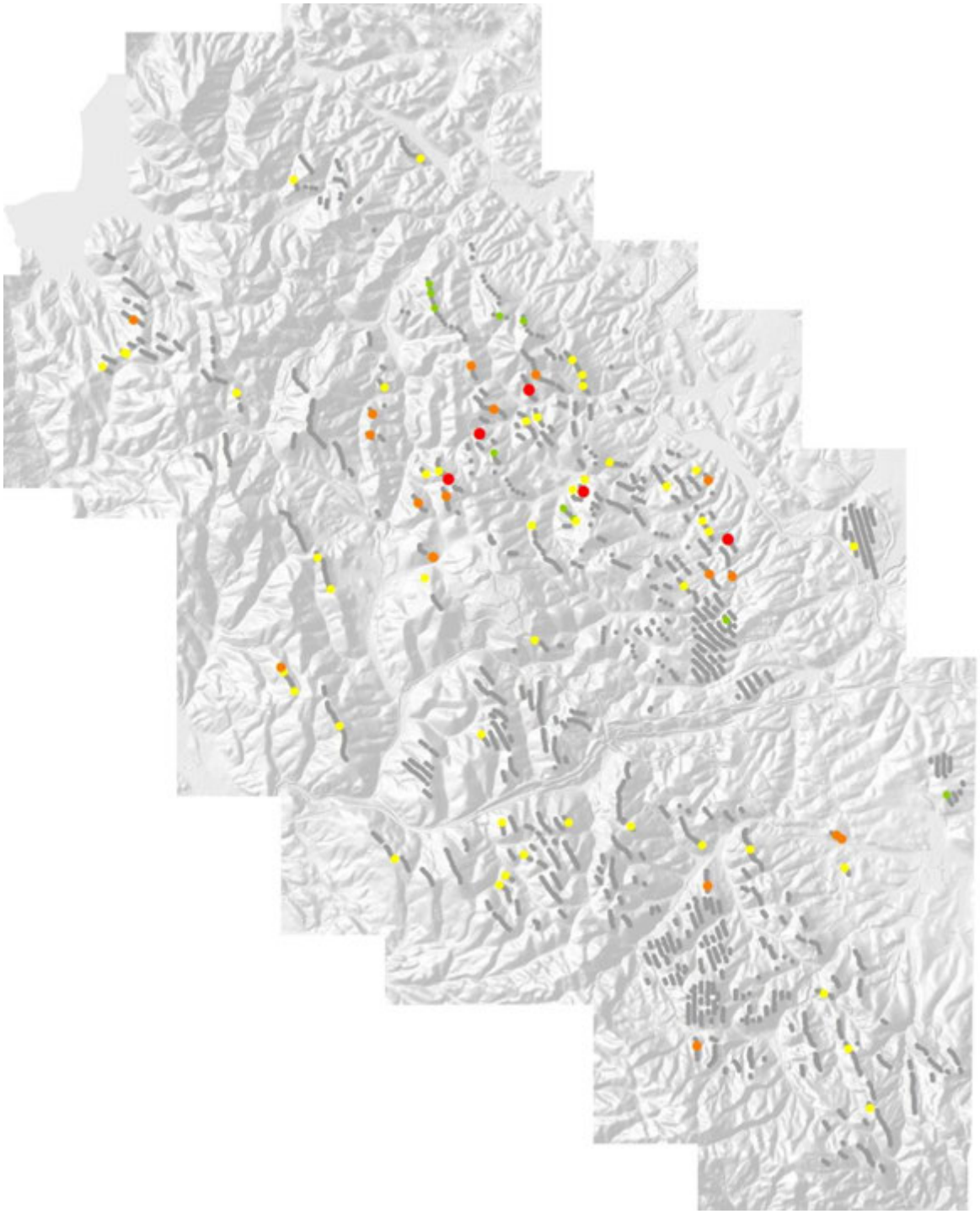

Figure 16. *Golden eagle fatality rates at Altamont Pass wind turbines adjusted for the duration of monitoring where gray circles represent wind turbines where eagle fatalities were not found and colored circles represent adjusted fatality rates from lowest (yellow) to highest (red).*

Digital Elevation Model

Two separate digital elevation model (DEM) grids were utilized for this project. The geoprocessing tasks were performed using a 10 foot cell size DEM created by combining DEMs obtained from Contra Costa and Alameda Counties. These data sets were produced using LIDAR data and ARC TIN software by Mapcon Mapping Inc. during 2007-2008. The border of the APWRA was used as a mask to produce the APWRA DEM composed of 25,440,000 10x10-foot cells. This DEM was then converted to a cell centroid point feature class and each point assigned a unique membership number.

All derived parameters were calculated for the entire APWRA DEM and attributed into the cell centroid point feature class. An aggregated 792-m buffer served as our mask (limit) for analyzing previously collected bird data against the DEM parameters. The 792-m radius was converted to a 2,600 foot radius and an additional 200 feet was added to buffer modeling data for geoprocessing and to ensure that all bird observations would be covered.

The statistical analyses within the APWRA were limited (masked) to data within the areas searched for raptors within the behavior study areas, bur burrowing owl burrows within the burrowing owl sampling plots, and for fatality rates among the wind turbines that were monitored at least one year (and the grid cells on which the turbines were located). The resulting analytical grids within the behavior survey areas were composed of a 7,548,578 (30%) subset of the 10x10-foot centroid point feature class serving as the study area for the behavior surveys, and a 393,555 subset serving as the study area for the behavior surveys restricted to 10-m buffered ridge-like features. These analytical grids were used to develop and test predictive models.

The same geoprocessing steps were used to characterize terrain attributes as reported in Smallwood and Neher (2010a,b). We used the Curvature function in the Spatial Analysis extension of ArcGIS 10.2 to calculate the curvature of a surface at each cell centroid. A positive curvature indicated the cell surface was upwardly convex, a negative curvature indicated the cell surface was upwardly concave, and zero indicated the cell surface was flat. Curvature data (-51 to 38) were classified using Natural Breaks (Jenks) with 3 classes of curvature – convex, concave and mid-range. Break values were visually adjusted to minimize the size of the mid-range class. A series of geoprocessing steps was used, called 'expand,' 'shrink,' and 'region group,' as well as 'majority filter tools' to enhance the primary slope curvature trend of a location. The result was a surface almost exclusively defined as either convex or concave (expressed as 1 or 0, respectively, for the variable *Curve*, and 2 and 1 respectively, for the variable *RidgeValley*, which will appear in the models below). Convex surface areas consisted primarily of ridge crests and peaks, hereafter referred to as ridges, and concave surface areas consisted primarily of valleys, ravines, ridge saddles and basins, hereafter referred to as valleys.

Line features representing the estimated average centers of ridge crests and valley bottoms were derived from the following steps. ESRI's Flow direction function was used to create a flow direction from each cell to its steepest down-slope neighbor, and then the Flow accumulation function was used to create a grid of accumulated flow through each cell by accumulating the weight of all cells flowing into each down-slope cell. A valley started where 50 upslope cells had contributed to it in the Flow accumulation function, and a ridge started where 55 cells

contributed to it. We applied flow direction and flow accumulation functions to ridges by multiplying the DEM by -2 to reverse the flow. Line features representing ridges and valley bottoms were derived from ESRI's gridline and thin functions, which feed a line through the centers of the cells composing the valley or ridge. Thinning put the line through the centers of groups of cells ≥40 in the case of valleys. Lines representing ridges and valleys were also clipped to identify the major valleys and major ridges, or the topographic features dominating the local skyline and local drainage systems (Figure 17).

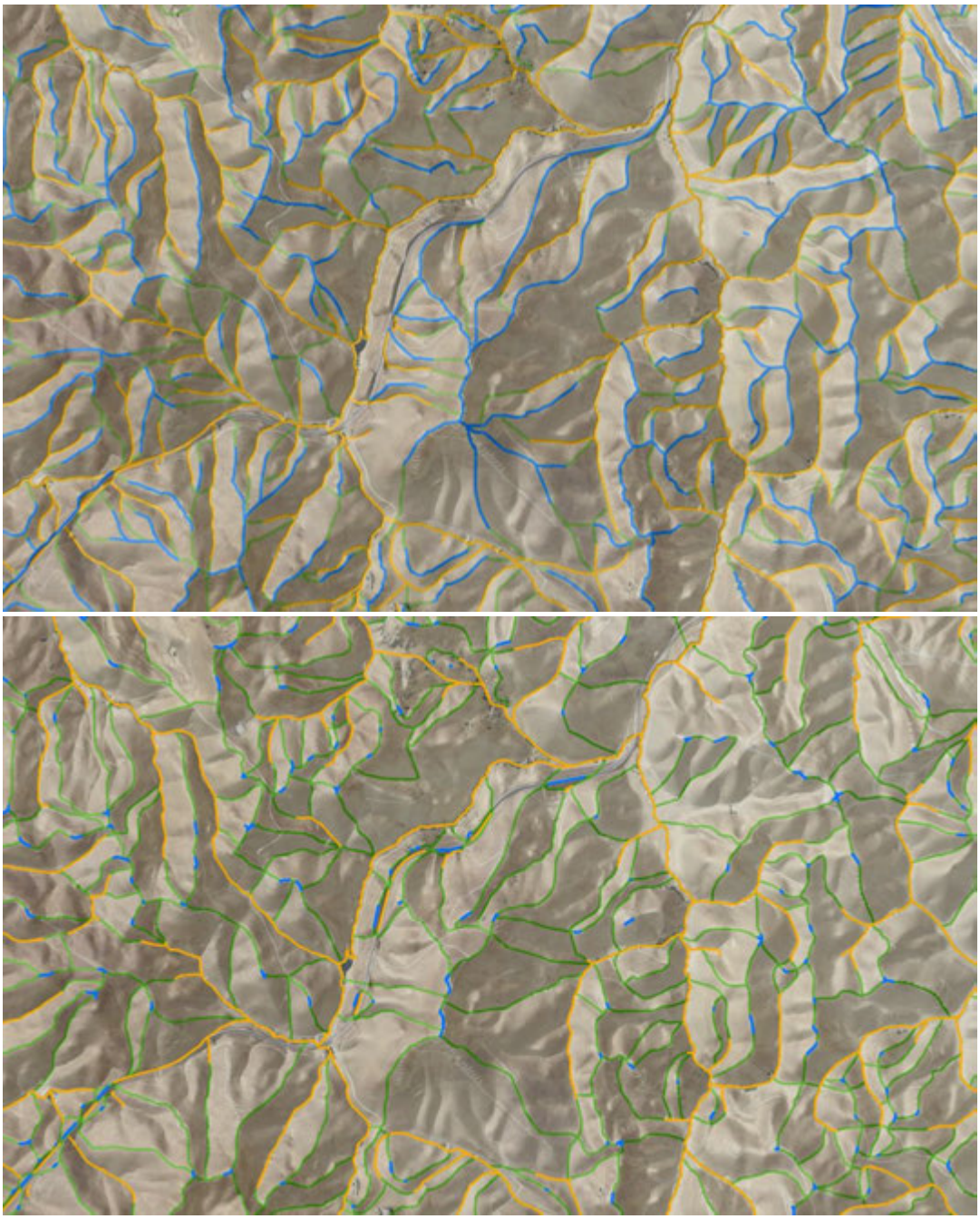

Figure 17. *Valley bottoms (gold) and ridge crests (blue) for all terrain (top) and major terrain (bottom) features*.

We used the two-foot slope analysis grid to create polygons with relatively gentle slope. We used a Standard Deviation classification to identify areas with < 7.4 % slope. These areas were then converted to polygons and intersected with the ridge/valley lines to determine polygons associated with either ridge or valley descriptions. The borders of these polygons were converted to lines and combined with the ridge/valley line datasets, respectively, and polygons in valley features were termed *valley polygons* and polygons on ridge tops were termed *ridge polygons*.

Horizontal distances (m) were then measured between each DEM grid cell and the nearest valley bottom boundary (in the valley line combined data set) and the nearest ridge top boundary or ridgeline (in the ridgeline combined data set), referred to as *distance to valley* and *distance to ridge*, respectively. These distances were measured from the DEM grid cell to the closest grid cell of a valley bottom or ridgeline, respectively, not including vertical differences in position. The *total slope distance* was the sum of *distance to valley* and *distance to ridge*, and expressed the size of the slope. The DEM grid cell's position in the slope was also expressed as the ratio of *distance to valley* and *distance to ridge*, referred to as the *distance ratio*. This expression of the grid cell's position on the slope removed the size of the slope as a factor. The same measurements were made to major valleys and major ridges.

The vertical differences between each DEM grid cell and the nearest valley bottom boundary and nearest ridge top boundary or ridgeline were referred to as *elevation difference*, and this measure also expressed the size of the slope. In addition to the trend in slope grade at each DEM grid cell, the *gross slope* was measured as the ratio of *elevation difference* and *total slope distance*. The DEM grid cell's position on the slope was also expressed as the ratio of the elevation differences between the grid cell and the nearest valley and between the grid cell and the nearest ridge, referred to as *elevation ratio*. Additionally, the grid cell's position on the slope was measured as the average of the percentage distance and the percentage elevation to the ridge top. This mean percentage was named *percent up slope*, and provided a more robust expression of the grid cell's position on the slope (Figure 18). The same measurements were made to major valleys and major ridges, leading to the variable we named *percent up major terrain slope*. Thus, on a small hill adjacent to a major hill in the area, a grid cell could be 90% under *percent up slope* and only 30% under *percent up major terrain slope*.

Percent up slope did not distinguish a grid cell's position between slopes on large hills versus medium or small-sized hills, so the local topographic influence of the feature where each cell was located was expressed by the variable *hill size*, which was the elevation difference between the nearest valley bottom polygon and nearest prominent ridge top polygon. *Major hill size* was the elevation difference between the nearest major valley bottom and nearest major ridge top.

Breaks in slope were characterized with the ratio of *slope to gross slope*, and the ratio *gross slope to major gross slope* was also calculated. Additional ratios included *local to major hill size*, *local to major ridge elevation*, and *local to major valley elevation*.

Each DEM grid cell was classified by *aspect* according to whether it faced north, northeast, east, southeast, south, southwest, west, northwest, or if it was on flat terrain. Each grid cell was also

categorized as to whether its center on the landscape was windward, leeward or perpendicular to the prevailing southwest and northwest wind directions as recorded during the behavior observation sessions.

The study area was divided into smaller polygons of land with like aspect, creating a predictor variable termed *Subwatershed Orientation*. Existing sub-watershed polygons already had been created between ridgelines and valley bottom lines. These watershed polygons were further divided by reviewing the existing 2-foot hypsography (contour) data and then dividing them into orientation polygons where the overall orientation of the contours changed. An orientation line feature layer was digitized with a line for each new polygon following the best observed orientation of that polygon's contours. Python scripts attributed the new line with its compass orientation, e.g., N, NNE, NE. These lines were non-directional, so a compass value could be either the returned value or the direction 180 degrees opposite. These same scripts calculated a perpendicular compass direction to the returned orientation line direction. The perpendicular orientation direction had two possible values, differing by 180 degrees based on which side of the ridge the line described. A reference point within each orientation polygon was georeferenced by scripts to a generalized aspect grid of the study area. The scripts determined the correct perpendicular orientation and calculated the compass direction of the orientation polygon.

Using similar steps, a predictor variable termed *Ridge Orientation* was created. Ridgelines were buffered by 10 feet and the resulting ridgeline polygons classified by orientation: north to south, north-northwest to south-southeast, northwest to southeast, west-northwest to east-southeast, west to east, west-southwest to east-northeast, southwest to northeast, and south-southwest to north-northeast. Flight paths crossing ridgelines were related to these Ridge Orientation polygons in use and availability analysis.

Steps to identify saddles, notches, and benches

Because a large amount of evidence links disproportionate numbers of raptor fatalities to wind turbines located on aspects of the landscape that are lower than immediately surrounding terrain or that represent sudden changes in elevation, a special effort was directed toward identifying ridge saddles, notches in ridges, and benches of slopes. Benches of slopes are where ridge features emerge from hill slopes that extend above the emerging ridge. These types of locations are where winds often compress by the landscape to create stronger force, and where raptors typically cross hilly terrain or spend more time to forage for prey. Compared to surrounding terrain, these types of features are often relatively flatter or shallower in slope and sometimes include lower elevations (e.g., saddles). Geoprocessing steps were used to provide some objectively to the identification of these features, but judgment was also required because conditions varied widely in how such features were formed and situated.

The same procedures were used as used in the ridge/valley selection. The two foot slope analysis grid was used to create polygons with a relatively gentle slope. A Standard Deviation classification was used to identify areas with < 7.4 % slope. These areas were then converted to polygons. Those polygons not associated with ridge or valley polygons were examined manually. Where these polygons were visually associated with saddle and or step features, they

were identified as *hazard sites* representing saddles, notches, or benches. Maps depicting contours of the variable *percent up slope* were also examined, because these contours readily revealed sudden breaks in slope typical of saddles, notches, and benches, which were then also represented with polygons.

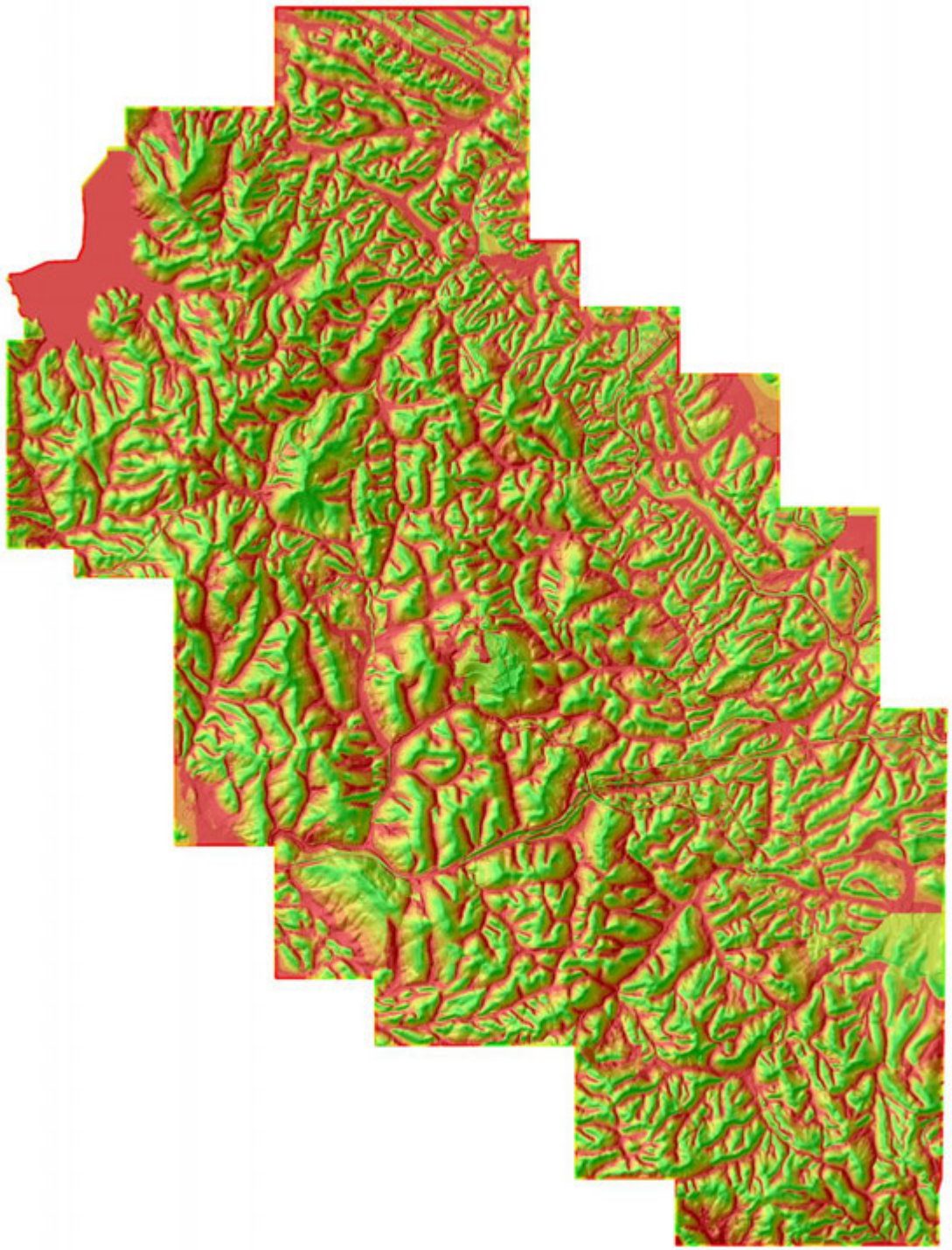

Figure 18. *Percent up slope across the Altamont Pass Wind Resource Area was derived from multiple terrain measurements to express a grid cell's position on the slope regardless of the size of the slope, where red was at the valley bottoms and dark green at the ridge crests*.

GPS/GSM Telemetry

Doug Bell (2015) caught 18 golden eagles using baited traps since 18 December 2012. To each eagle he affixed 70 g GPS/GSM units manufactured by Cellular Tracking Technologies, LLC (CTT; http://celltracktech.com/) via backpack harness. CTT units measure 100 mm x 40 mm x 23 mm and run on solar powered batteries during daylight hours (Figure 19). All units recorded positions at 15 min intervals, and a subset recorded positions at 30 sec intervals during 3 days of every month. Actual times between position intervals vary, but are supposed to average 15 min or 30 sec. CTT Transmitters download data to cell towers daily during prescribed 1 hour windows, but if a transmitter is beyond cell tower coverage, it will store location data until it returns to an area with cell coverage. Eagle location data are down-loaded from the CTT website, and are password protected.

Figure 19. *A golden eagle fitted with a GPS/GSM telemetry unit as seen during a visual scan survey to record behavior patterns*.

GPS/GSM telemetry positions were collected from all telemetered golden eagles intersecting the boundary of the APWRA from the inception of telemetry monitoring through November 2015. Lines representing flight paths were derived by connecting sequential positions, so each line was associated with a distance and time interval summed among all line segments, where a line segment was the line connecting two sequential positions. New flight lines were initiated each day, as well as when time intervals between sequential positions exceeded 60 sec in the case of data collected at 30 sec intervals and 1,020 sec in the case of data collected at 15 min (900 sec) intervals. We also subsampled 15 min interval data from 30 sec data was when the accumulated time among sequential positions surpassed 900 sec. We included the subsampled 15 min data with the 15 min interval data.

To assess error in the GPS/GSM telemetry units we placed these units on the ground for long periods next to a Trimble GeoXT with sub-meter accuracy. We also mounted telemetry units in the back of Smallwood's truck (1.2 m above ground) and next to a Trimble GeoXT unit while driving throughout the APWRA on various dates from 22 October 2014 through 10 September 2015. Our visual examination of the GPS/GSM data indicated high lateral position accuracy relative to the Trimble GeoXT unit. However, we noticed high vertical error and a large vertical bias in the GPS/GSM data when examining simple statistics and histograms. Whereas the Trimble GeoXT unit generated positions that averaged about a meter above the 10-foot DEM surface – where the average was supposed to be – the GPS/GSM data averaged 9 m below the 10-foot DEM surface. We therefore adjusted upward the vertical positions of the telemetered golden eagles by 9 m. We also generated a cumulative distribution curve of the vertical error in the truck-mounted telemetry data, and found that 95% of the recorded positions were within 27 m of their true positions above the 10-foot DEM surface (Figure 20). We therefore used 27 m as a threshold value for determining whether flight lines of golden eagles were above ground. Flight lines were assigned to the following height domains above our 10-foot DEM: **0 (ground)** was <0 m above the DEM surface, **1 (near ground)** = 0 to 27 m above the DEM, **2 (medium)** was >27 m and <200 m above the DEM, and **3 (high)** was >=200 m above the DEM.

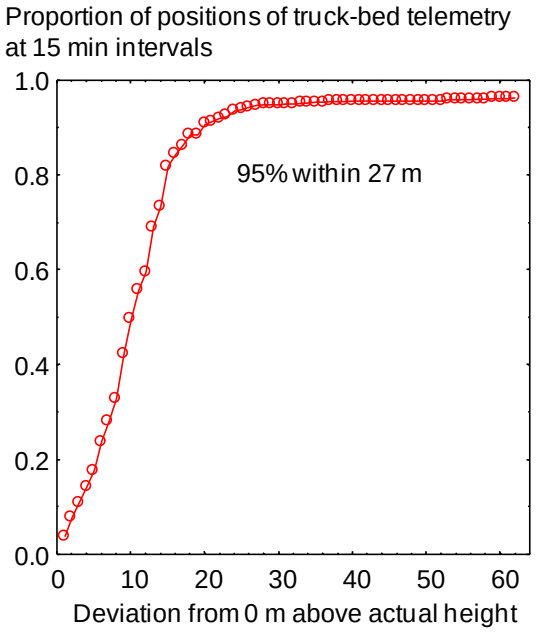

Figure 20. *Cumulative distribution of vertical error measured from 767 GPS/GSM telemetry positions between two units mounted in the back of Smallwood's truck at 1.2 m above ground while driving throughout the APWRA on various dates from 22 October 2014 through 10 September 2015.*

Examining data from GPS/GSM transmitters that we maintained at known locations (not affixed to eagles), we averaged false flight speeds caused by position scatter as 0.3 m/s (1.08 km/hr) for 30 second interval data, and 0.007 m/s (0.026 km/hr) for 15 min interval data. However, relying on speed alone was often insufficient for determining whether an eagle was flying because hovering or kiting golden eagles could have remained in the same locations over 30 sec intervals,

and flying golden eagles could have returned to the same positions after flying out and back to another location or in a circle (these behaviors have been seen during visual surveys many times).

Whether an eagle was flying was determined as **possible (0)** if the flight line averaged slower than the speed of position scatter and ≤0 m above the DEM and intersected 1 subwatershed polygon, or it averaged slower than the speed of position scatter and <200 m above the DEM and intersected 1 subwatershed polygon. Whether an eagle was flying was determined as **probable (1)** it the flight line averaged faster than position scatter and ≤27 m above the DEM and intersected ≥2 subwatershed polygons, or it averaged ≥3 km/hr and 0-27 m above the DEM and intersected ≥1 subwatershed polygon, or it averaged ≥1.08 km/hr and 27-200 m above the DEM and intersected ≥1 subwatershed polygon. Whether an eagle was flying was determined as **certain (2)** if the flight line averaged ≥2.5 km/hr or ≥100 m above the 10-foot DEM and intersected ≥4 subwatershed polygons, or it averaged ≥27 m above the DEM and intersected ≥3subwatershed polygons, or it averaged ≥2.3 km/hr and ≥27 m above the DEM and intersected ≥1subwatershed polygon. To prevent flight lines used in our association analysis from being falsely generated from position scatter around perched birds, we included lines determined to have been within height domains 1 or 2 and determined to have been certainly flying (2).

Associations between bird behaviors and terrain attributes

The location of each raptor was characterized by aspect, slope, rate of change in slope, direction of change in slope, and elevation. These variables were also used to generate raster layers of the study area, one raster expressing the aspect of the corresponding slope (hereafter referred to as *aspect*), and the other expressing whether the landscape feature was tending toward convex versus concave orientation (expressed in a variable named *curve*). These features were defined using geoprocessing.

Fuzzy logic (FL) modeling (Tanaka 1997) was used to predict the likelihood each grid cell would be used by golden eagle, red-tailed hawk, American kestrel, and burrowing owl. FL likelihood surfaces were first created by each selected predictor variable. The mean, standard deviation, and standard error were calculated for each predictor variable among the grid cells where each targeted bird species was observed during standard observation sessions. These statistics formed the basis from which FL membership was assigned to grid cells. Depending on the pattern in the data, FL membership was assigned values of 1 whenever the value of the predictor variable was within a certain prescribed distance in value from the mean, oftentimes within 1 SD, but sometimes within 1 or 2 SE. FL membership values of 1 expressed confidence that grid cells with the corresponding value range for the predictor variable are likely to be visited by the target species. FL membership values of 0 were assigned to grid cells that were far from the mean value, usually defined by prescribed distances from the mean such as >2 SD from the mean. FL membership values of 0 expressed confidence that grid cells with the corresponding value range for the predictor variable are unlikely to be visited by the target species. All other grid cells were assigned FL membership values according to the following formulae, assuming that the likelihood of occurrence of each species will grade gradually rather than abruptly across grid cells that vary in value of the predictor variable (Y):

$$0.5 \times (1 - \cos(\pi \times (Y - V_c) \div (V_f - V_c))) \text{ below the mean}$$
$$0.5 \times (1 + \cos(\pi \times (Y - V_c) \div (V_f - V_c))) \text{ above the mean,}$$

where V_c represented the variance term (SD or SE) closer to the mean and V_f represented the variance term farther from the mean.

FL likelihood values were then summed across predictor variables contributing to a species-specific model. In earlier efforts to develop FL models for golden eagle, red-tailed hawk, American kestrel and burrowing owl in other parts of the APWRA, natural breaks were used to divide the summed values into 4 classes, but the percentages of study area composing these classes remained consistent despite use of natural breaks. Therefore, this time the class divides were established at 63.5%, 83.5%, and 95.5%. Class 1, including FL likelihood values <63.5% (i.e., 63.5% of the study area), represented the suite of grid cells including fewer bird observations other than expected. Class 2, including FL likelihood values between 63.5% and 83.5% (i.e., 20% of the study area), represented the suite of grid cells including about equal or slightly greater than equal bird observations other than expected. Class 3, including FL likelihood values between 83.5% and 95.5% (i.e., 12% of the study area), represented the suite of grid cells including more bird observations other than expected. And class 4, including the upper 4.5% of FL likelihood values, represented the suite of grid cells including substantially more bird observations other than expected.

The performance of each model was assessed by the magnitude of the ratio of the observed number to the expected number of observations representing a dependent variable and occurring within the suite of conditions specified by each FL surface class. Dependent variables included fatality rates (except for American kestrel), flights <180 m above ground, flights across ridge features and <180 m above ground (Figure 21), social interactions while flying (Figure 22), wind turbine interaction events (Figures 23 and 24), and hovering or kiting or surfing behaviors (Figure 25). FL surface models were later projected across wind project areas.

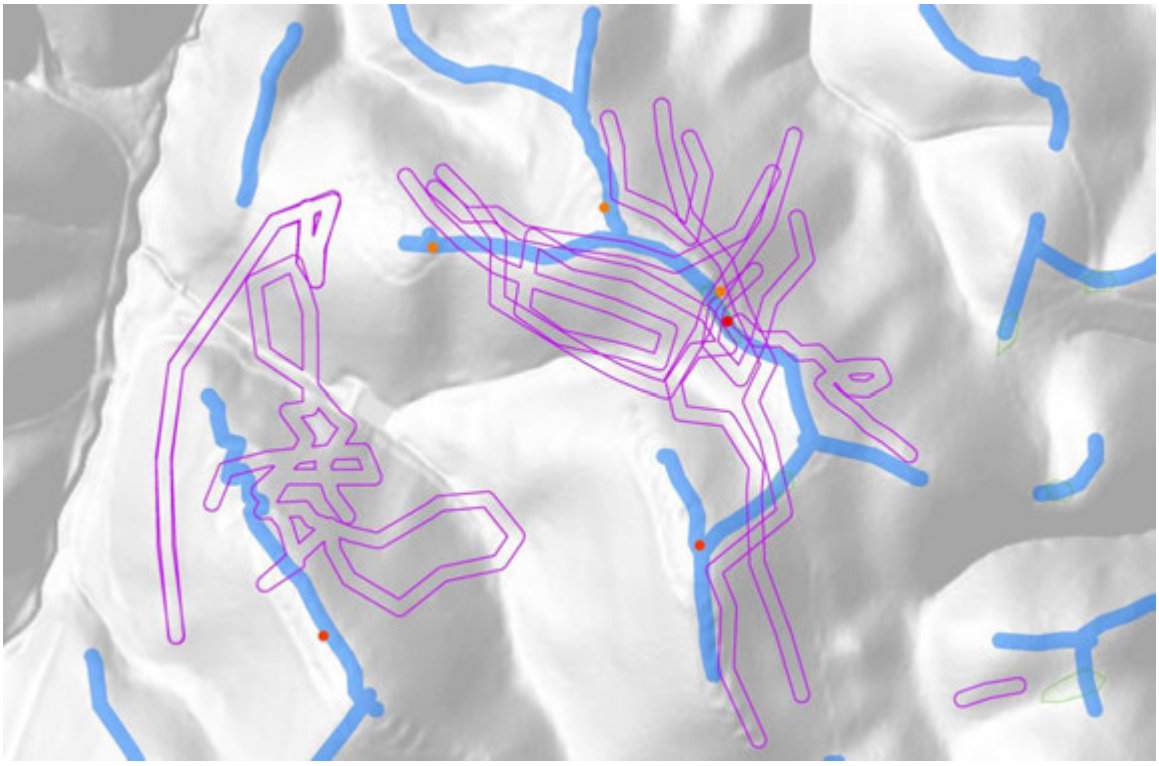

Figure 21. *Example of how golden eagle ridge crossings were quantified. WE buffered flights within 180 m of the ground by 10 m (purple polygons) and their overlap with 10-m buffered ridge crests (blue polygons) were counted for each ridge orientation: N-S, NNE-SSW, NE-SW, ENE-WSW, E-W, ESE-WNW, SE-NW, and SSE-NNW. Colored circles depict golden eagle fatality rates adjusted for monitoring duration, were red was the highest fatality rates.*

Figure 22. *Social or competitive interactions between flying birds served as a dependent variable for collision hazard modeling, so associations were sought between interacting birds and terrain measurements and terrain features.*

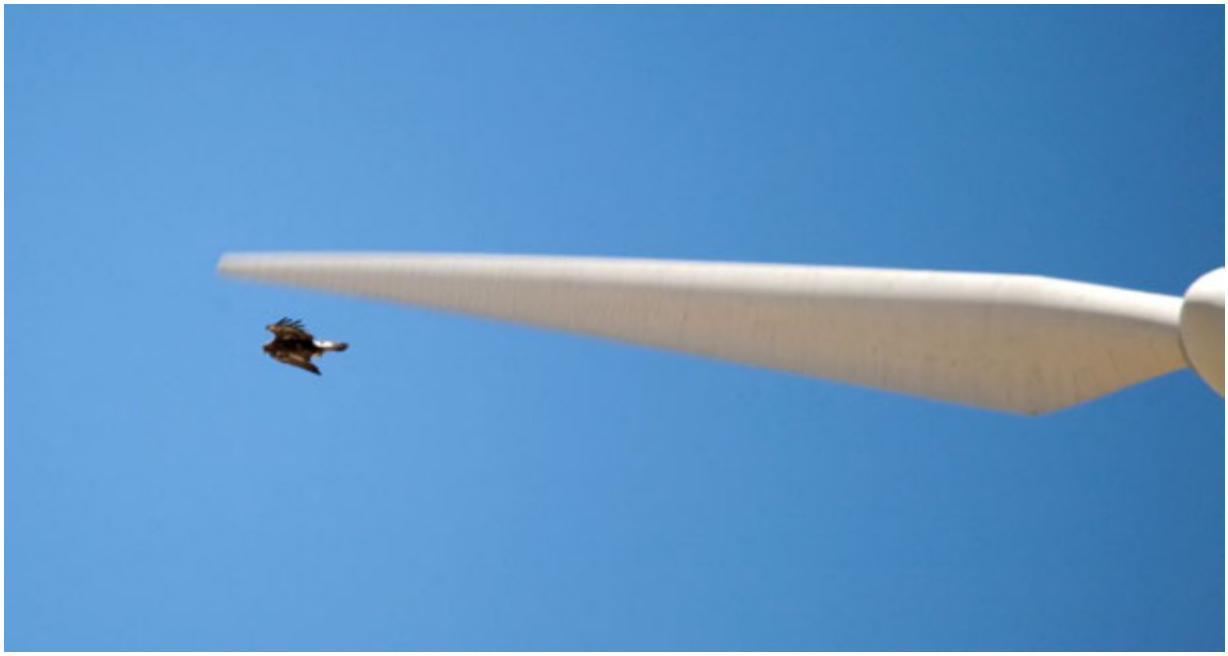

Figure 23*. Wind turbine events of birds adjudged by observers to have flown dangerously close to wind turbine blades were recorded and used for collision hazard modeling, so associations were sought between wind turbine events and terrain measurements and terrain features. In this case a golden eagle narrowly avoided a collision with a moving wind turbine blade.*

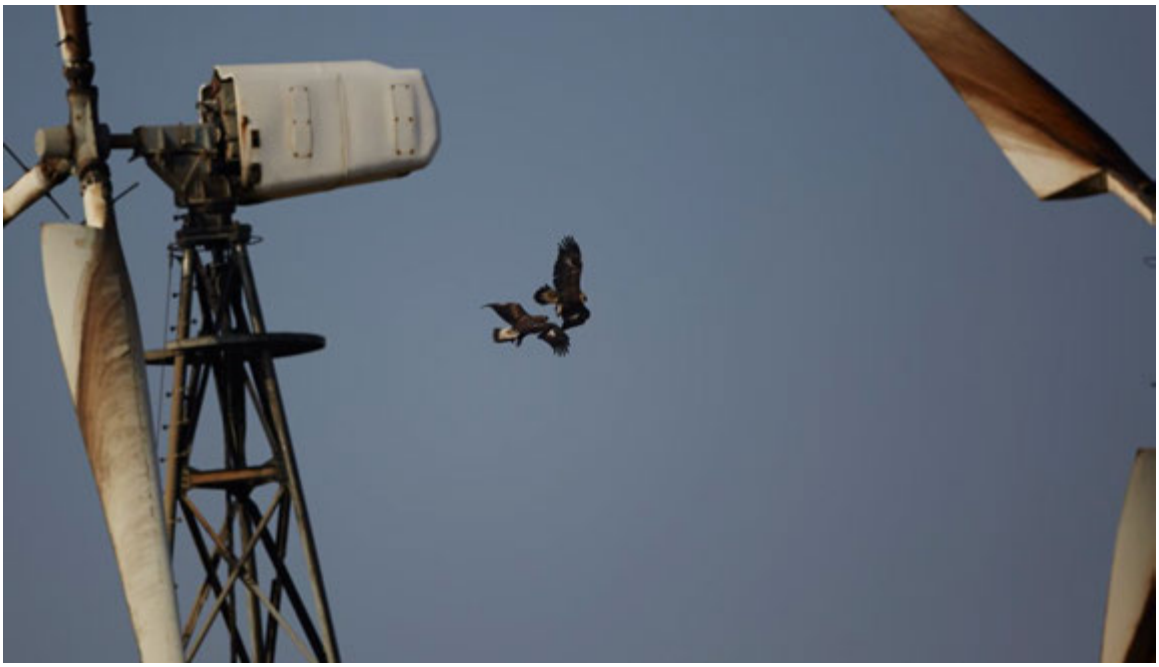

Figure 24*. Example of a social interaction between flying golden eagles that also happen to be near wind turbines. Where and under what conditions these combined social interactions and wind turbine events occur can assist with predicting collision hazard, but many hours of directed behavior surveys are needed to accumulate a sufficient number of these events to reliably associate them with environmental and terrain factors.*

Figure 25*. Red-tailed hawks kiting near the top of a slope. Red-tailed hawks, American kestrels and burrowing owls (at night) often perform this behavior just upwind of wind turbines. It is a known dangerous behavior, having preceded multiple eye-witness accounts of birds drifting with the wind or being pushed back by wind into operating wind turbine rotors. The behavior is also dangerous because kiting or hovering birds often break off from these behaviors to glide quickly with the wind before turning back into the wind to repeat the behaviors over another portion of the slope, but the glide with the wind often places them in sudden jeopardy of colliding with turbine blades*.

Burrowing owl model

Because burrowing owls tend to nest low on the slope, it would be rare for a predictive model of burrowing owl burrow locations to correspond with terrain where burrowing owls are killed by wind turbines. Therefore, we developed a burrowing owl fatality model and relied on hazard classes 3 and 4 of this model wherever the cell centroids were located within 60 m of classes 3 or 4 predicted by the burrow model. Otherwise, all class values of the burrow model remained unchanged.

RESULTS

GPS/GSM Telemetry of Golden Eagles

All 18 of the golden eagles fitted with GPS/GSM telemetry units intersected the APWRA at some point during the study (Figure 26). Two of the eagles barely overlapped the APWRA with 3 positions each, so they did not contribute anything to the analysis. Another two eagles recorded only 15 and 16 positions within the APWRA, so they, too, contributed little if anything to the analysis. The other 14 eagles contributed hundreds or thousands of positions within the APWRA.

Our examination of associations between eagle positions and terrain variables indicated no difference between eagles tracked at 30 sec intervals and those tracked at 15 min intervals. Therefore, we combined the data from the two position intervals for quantifying associations with terrain variables. We found high variation in terrain associations between gender and age classes of eagles, but none of this variation appeared meaningful. However, we noticed strong differences in terrain associations between the 3 eagles that collided with wind turbines versus those that have not yet collided with wind turbines. Therefore, we relied mostly on terrain associations of the 3 eagles that collided with wind turbines to develop a collision hazard model.

After combining data sets based on 30 sec and 15 min intervals, golden eagle telemetry positions adjusted for vertical bias and intersecting the APWRA numbered 17,025 (14%) at or below ground (of course, these birds were not truly below ground, but recorded below ground due to position errors), 79,757 (66%) near ground, 18,396 (15%) within the hazardous height zone of 27 m to 200 m above ground, and 6,079 (5%) high above ground. Of the golden eagle positions intersecting the APWRA, 1.39% were possibly of flying eagles, 12.88% were probably of flying eagles, and 85.73% were certainly of flying eagles.

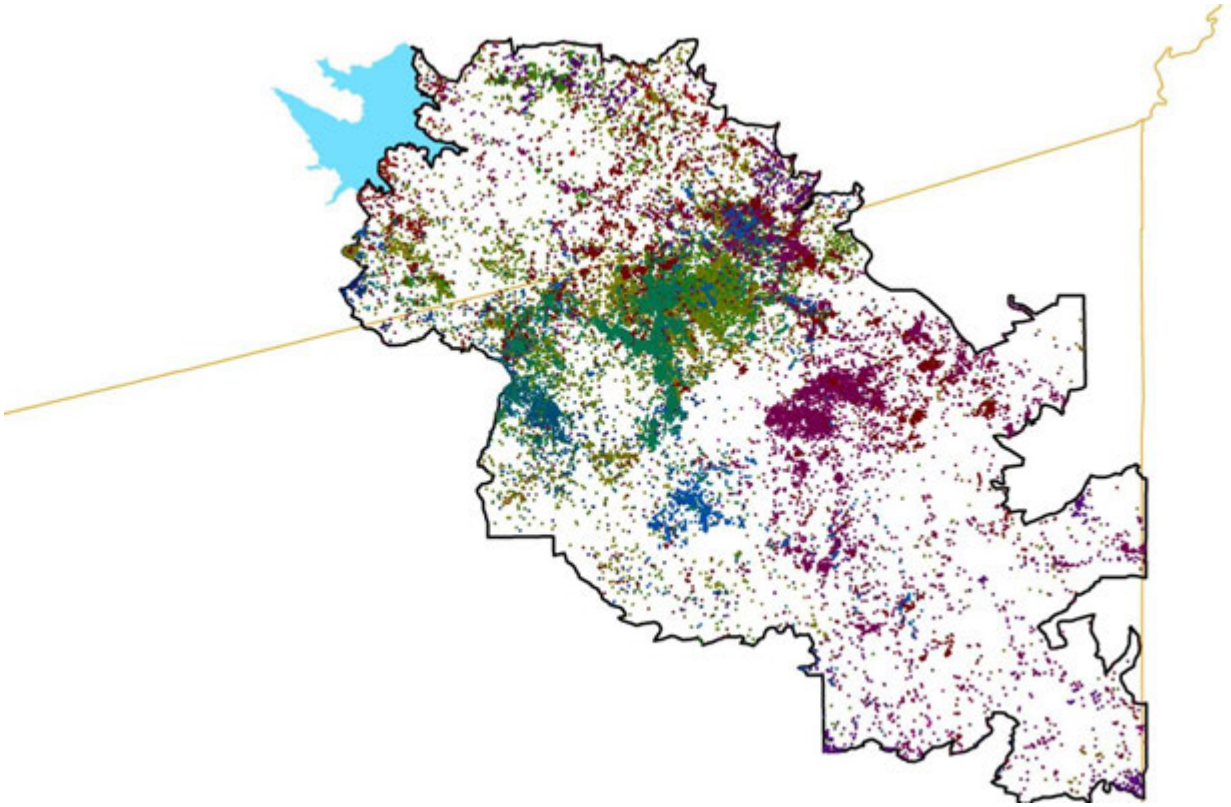

Figure 26. *GPS/GSM telemetry positions of golden eagles (each color represents a different eagle) within the boundary of the Altamont Pass Wind Resource Area, December 2012 through September 2015. Orange lines represent County boundaries, and the blue polygon at the upper left is Los Vaqueros Reservoir*.

Visual Surveys

Behavior surveys performed at Sand Hill through 5 April 2015 numbered 2,002 30-min surveys and across the rest of the APWRA through 29 October 2015 numbered 1,095 1-hr surveys elsewhere in the APWRA for a combined 2,096 hours. Observers recorded 1,065 golden eagle flights, 2,368 red-tailed hawk flights, and 706 American kestrel flights. The rate of flights were 0.2845 golden eagles/hour, 0.9366 red-tailed hawks/hour, and 0.4827 American kestrels/hour at Sand Hill sites, and 0.9938 golden eagles/hour, 1.8543 red-tailed hawks/hour, and 0.3151 American kestrels/hour elsewhere in the APWRA. APWRA-wide observation rates were 0.6115 golden eagles/hour, 1.3597 red-tailed hawks/hour, and 0.4054 American kestrels/hour. We recorded events at wind turbines, including 86 golden eagle events, 156 red-tailed hawk events, and 98 American kestrel events.

Hazard Models

The FL models of golden eagle were composed of 7 predictor variables based on telemetry data (Table 1), 5 predictor variables based on behavior data (Table 2), and 4 predictor variables based on fatality rates (Table 3). The FL models of red-tailed hawk were composed of 4 predictor variables based on behavior data (Table 4), and 4 predictor variables based on fatality rates (Table 5). The FL models of American kestrel were composed of 7 predictor variables based on behavior data (Table 6), but no measured variables predicted fatality rates. The FL models of burrowing owl were composed of 2 predictor variables based on burrow location data (Table 7), and 4 predictor variables based on fatality rates (Table 8). How the models were weighted and combined for each species is summarized in Table 9.

Telemetered golden eagles were recorded flying disproportionately over the upper portions of slopes, even more so for the colliders (Figure 27). Colliders were also disproportionately recorded flying higher up the slopes of major terrain features, as well as over ridges oriented east to west and east-southeast to west-northwest and over slopes facing north-northwest, south-southwest and south (Figure 28). Colliders were disproportionately recorded flying farther from the major valley bottoms and over steeper-than-average slopes.

Golden eagle flights and wind turbine interactions occurred disproportionately over ridges oriented generally west-east. Associations were also strong with subwatershed slopes facing westerly directions, especially west and north-northwest. Golden eagles flew and interacted with wind turbines disproportionately at 91% to 100% up the slope, and at 45% to 100% up the slope of major terrain features (Figure 29).

Red-tailed hawks hovered and kited disproportionately over ridges oriented west to east and north-northwest to south-southeast. They hovered and kited disproportionately over slopes oriented southwest, west-southwest and west. Red-tailed hawks hovered and kited disproportionately over ground that was between 85% and 100% to the top of the slope (Figure 30). Red-tailed hawk kiting and hovering was broader across major terrain features, with peak activity ranging between 53% and 83% to the top of the feature (Figure 30).

American kestrels flew most disproportionately over ridges oriented west-east, north-south, and northwest to southeast. American kestrels flew disproportionately over slopes oriented west and southwest, ranging mostly between three-quarters to the peak of the slope and midway to just below the peaks of major terrain features.

Burrowing owl burrows were located disproportionately between 5% and 30% of the way up south-facing slopes (Figure 31). Burrowing owl fatality rates were disproportionately higher at low to moderate elevations and between 35% and 42% of the way up the slopes of major terrain features and in hazard sites (Figure 31).

Map-based collision hazard models were used to recommend shifts in the initially proposed wind turbine layout at Sand Hill (Figures 32-35). These models were combined from other models as described in the Methods section and Table 9).

Table 1. *Golden eagle fuzzy logic membership functions of DEM grid cells based on GPS telemetry positions primarily of 3 study birds that collided with wind turbines.*

Value of variable Y for *i*th grid cell (type of event)	**Membership function of grid cell (Values >1 include weightings)**
Ridge Orientation	
Y = W-E	3
Y = WNW-ESE	2
Y = NW-SE,	1
Y = Other orientation	0
Subwatershed Orientation	
Y = S, SSW, NNW	2
Y = N, NE, SW, WNW	1
Y = Other orientation	0
Percent up slope	
$85.70 < Y \leq 100$	1
$71.56 \leq Y \leq 85.70$	$0.5 \times (1 - \text{COS}(\pi \times (Y - 71.56) / (85.70 - 71.56)))$
$Y < 71.56$	0
Percent up major terrain slope	
$59.0 < Y \leq 98.0$	1
$39.5 \leq Y \leq 59.0$	$0.5 \times (1 - \text{COS}(\pi \times (Y - 39.5) / (59.0 - 39.5)))$
$98.0 < Y \leq 100.0$	$0.5 \times (1 + \text{COS}(\pi \times (Y - 98.0) / (100.0 - 98.0)))$
$Y < 39.5$	0
Distance to Major Valley	
$168.81 < Y \leq 538.34$	1
$117.25 \leq Y \leq 168.81$	$0.5 \times (1 - \text{COS}(\pi \times (Y - 117.25) / (168.81 - 117.25)))$
$538.34 < Y < 684.44$	$0.5 \times (1 + \text{COS}(\pi \times (Y - 538.34) / (684.44 - 538.34)))$
$Y < 117.25$ or $Y > 684.44$	0
Gross slope	
$19.56 < Y \leq 33.10$	1
$15.04 \leq Y \leq 19.56$	$0.5 \times (1 - \text{COS}(\pi \times (Y - 15.04) / (19.56 - 15.04)))$
$33.10 < Y < 42.13$	$0.5 \times (1 + \text{COS}(\pi \times (Y - 33.10) / (42.13 - 33.10)))$
$Y < 15.04$ or $Y > 42.13$	0
Hazard site	
Y = Within polygon	1
Y = Outside polygon	0

Table 2. *Golden eagle fuzzy logic membership functions of DEM grid cells based on flights involving ridge crossings, interactions with other birds, and wind turbine interaction events.*

Value of variable Y for *i*th grid cell (type of event)	**Membership function of grid cell (Values >1 include weightings)**
Ridge Orientation (ridge crossings, social interactions, turbine events, behavior)	
Y = W-E	3
Y = N-S, NE-SW, NNW-SSE	1
Y = NW-SE, WNW-ESE	0.5
Y = Other orientation	0
Subwatershed Orientation (social interactions, turbine events, behavior)	
Y = W, NNW	2
Y = NW, WSW, SSW	1
Y = Other orientation	0
Percent up slope (social interactions)	
$91.80 < Y \leq 100$	1
$75.19 \leq Y \leq 91.80$	$0.5 \times (1 - \text{COS}(\pi \times (Y - 75.19) / (91.80 - 75.19)))$
$Y < 75.19$	0
Percent up major terrain slope (turbine events)	
$72.10 < Y \leq 100$	1
$48.95 \leq Y \leq 72.10$	$0.5 \times (1 - \text{COS}(\pi \times (Y - 48.95) / (72.10 - 48.95)))$
$Y < 48.95$	0
Hill Size (social interactions)	
$74.24 < Y \leq 89.13$	1
$19.65 \leq Y \leq 74.24$	$0.5 \times (1 - \text{COS}(\pi \times (Y - 19.65) / (74.24 - 19.65)))$
$89.13 < Y < 94.09$	$0.5 \times (1 + \text{COS}(\pi \times (Y - 89.13) / (94.09 - 89.13)))$
$Y < 19.65$ or $Y > 94.09$	0

Table 3. *Golden eagle fuzzy logic membership functions of DEM grid cells based on fatality rates at wind turbine locations.*

Value of variable Y for *i*th grid cell (type of event)	**Membership function of grid cell (Values >1 include weightings)**
Ridge elevation	
$219.84 < Y \leq 273.88$	1
$70.60 \leq Y \leq 219.84$	$0.5 \times (1 - COS(\pi \times (Y - 70.60) / (219.84 - 70.60)))$
$273.88 < Y \leq 423.12$	$0.5 \times (1 + COS(\pi \times (Y - 273.88) / (423.12 - 273.88)))$
$Y < 70.60$ or $Y > 423.12$	0
Major valley elevation	
$160.36 < Y \leq 211.41$	1
$102.62 \leq Y \leq 160.36$	$0.5 \times (1 - COS(\pi \times (Y - 102.62) / (160.36 - 102.62)))$
$211.41 < Y \leq 269.16$	$0.5 \times (1 + COS(\pi \times (Y - 211.41) / (269.16 - 211.41)))$
$Y < 102.62$ and $Y > 269.16$	0
Slope to grosslope ratio	
$0.36 < Y \leq 0.49$	1
$0.08 \leq Y \leq 0.36$	$0.5 \times (1 - COS(\pi \times (Y - 0.08) / (0.36 - 0.08)))$
$0.49 < Y < 0.77$	$0.5 \times (1 + COS(\pi \times (Y - 0.49) / (0.77 - 0.49)))$
$Y < 0.08$ or $Y > 0.77$	0
Hazard site	
Y = Within polygon	1
Y = Outside polygon	0

Table 4. *Red-tailed hawk fuzzy logic membership functions of DEM grid cells based on flights involving ridge crossings, interactions with other birds, behavior, and wind turbine interaction events.*

Value of variable Y for *i*th grid cell (type of event)	**Membership function of grid cell (Values >1 include weightings)**
Ridge Orientation (ridge crossings, social interactions, turbine events, hovering/kiting)	
Y = W-E, SSW-ENE	2
Y = N-S, NNW-SSE	1
Y = Other orientation	0
Subwatershed Orientation (ridge crossings, social interactions, turbine events, hovering/kiting)	
Y = WSW, W	3
Y = SW, NW	2
Y = N, NNE, WNW, NNW	1
Y = Other orientation	0
Percent up slope (hovering/kiting)	
$85.43 < Y \leq 100$	1
$43.84 \leq Y \leq 85.43$	$0.5 \times (1 - COS(\pi \times (Y - 43.84) / (85.43 - 43.84)))$
$Y < 43.84$	0
Percent up major terrain slope (hovering/kiting)	
$52.98 < Y \leq 82.66$	1
$29.24 \leq Y \leq 52.98$	$0.5 \times (1 - COS(\pi \times (Y - 29.24) / (52.98 - 29.24)))$
$82.66 < Y \leq 100$	$0.5 \times (1 + COS(\pi \times (Y - 82.66) / (100 - 82.66)))$
$Y < 29.24$	0

Table 5. *Red-tailed hawk fuzzy logic membership functions of DEM grid cells based on fatality rates at wind turbine locations.*

Value of variable Y for *i*th grid cell (type of event)	**Membership function of grid cell (Values >1 include weightings)**
Ridge elevation	
$199.06 < Y \leq 273.62$	1
$42.22 \leq Y \leq 199.06$	$0.5 \times (1 - COS(\pi \times (Y - 42.22) / (199.06 - 42.22)))$
$273.62 < Y \leq 430.45$	$0.5 \times (1 + COS(\pi \times (Y - 273.62) / (430.45 - 273.62)))$
$Y < 42.22$ or $Y > 430.45$	0
Elevation	
$166.42 < Y \leq 291.07$	1
$34.03 \leq Y \leq 166.42$	$0.5 \times (1 - COS(\pi \times (Y - 34.03) / (166.42 - 34.03)))$
$291.07 < Y \leq 423.46$	$0.5 \times (1 + COS(\pi \times (Y - 291.07) / (423.46 - 291.07)))$
$Y < 34.03$ and $Y > 423.46$	0
Major terrain percent upslope	
$45.34 < Y \leq 67.16$	1
$27.89 \leq Y \leq 45.34$	$0.5 \times (1 - COS(\pi \times (Y - 27.89) / (45.34 - 27.89)))$
$67.16 < Y < 84.63$	$0.5 \times (1 + COS(\pi \times (Y - 67.16) / (84.63 - 67.16)))$
$Y < 27.89$ or $Y > 84.63$	0
Hazard site	
Y = Within polygon	1
Y = Outside polygon	0

Table 6. *American kestrel fuzzy logic membership functions of DEM grid cells based on flights involving ridge crossings, interactions with other birds, behavior, and wind turbine interaction events.*

Value of variable Y for *i*th grid cell (type of event)	**Membership function of grid cell (Values >1 include weightings)**
Ridge Orientation (ridge crossings, social interactions, turbine events, hovering/kiting)	
Y = W-E, WNW-ESE	1
Y = Other orientation	0
Subwatershed Orientation (ridge crossings, social interactions, turbine events, hovering/kiting)	
Y = WSW, W, NW, NNW	2
Y = N, NNE, SE, SSE, SSW	1
Y = Other orientation	0
Percent up slope (hovering/kiting)	
$85.43 < Y \leq 100$	1
$43.84 \leq Y \leq 85.43$	$0.5 \times (1 - COS(\pi \times (Y - 43.84) / (85.43 - 43.84)))$
$Y < 43.84$	0
Percent up major terrain slope (hovering/kiting)	
$66.36 < Y \leq 92.55$	1
$40.15 \leq Y \leq 66.36$	$0.5 \times (1 - COS(\pi \times (Y - 40.15) / (66.36 - 40.15)))$
$92.55 < Y \leq 100$	$0.5 \times (1 + COS(\pi \times (Y - 92.55) / (100 - 92.55)))$
$Y < 40.15$	
Hill size (turbine events)	
$20.73 < Y \leq 25.03$	1
$9.98 \leq Y \leq 20.73$	$0.5 \times (1 - COS(\pi \times (Y - 9.98) / (20.73 - 9.98)))$
$25.03 < Y \leq 44.38$	$0.5 \times (1 + COS(\pi \times (Y - 25.03) / (44.38 - 25.03)))$
$Y < 9.98$ or $Y > 44.38$	0
Gross slope (turbine events)	
$7.11 < Y \leq 10.74$	1
$1.66 \leq Y \leq 7.11$	$0.5 \times (1 - COS(\pi \times (Y - 1.66) / (7.11 - 1.66)))$
$10.74 < Y \leq 22.55$	$0.5 \times (1 + COS(\pi \times (Y - 10.74) / (22.55 - 10.74)))$
$Y < 1.66$ or $Y > 22.55$	
Hazard site	
Y = Within polygon	1
Y = Outside polygon	0

Table 7. *Burrowing owl fuzzy logic membership functions of DEM grid cells based on burrow locations.*

Value of variable Y for *i*th grid cell (type of event)	**Membership function of grid cell (Values >1 include weightings)**
Subwatershed Orientation	
Y = S	2.5
Y = ESE, SE, SSE	1.5
Y = ENE, E	1
Y = Other orientation	0
Percent up slope	
$5.56 < Y \leq 20.83$	1
$0.47 \leq Y \leq 5.56$	$0.5 \times (1 - COS(\pi \times (Y - 0.47) / (5.56 - 0.47)))$
$20.83 \leq Y \leq 51.37$	$0.5 \times (1 + COS(\pi \times (Y - 20.83) / (51.37 - 20.83)))$
$Y < 0.47$ or $Y > 51.37$	0

Table 8. *Burrowing owl fuzzy logic membership functions of DEM grid cells based on fatality rates at wind turbine locations.*

Value of variable Y for *i*th grid cell (type of event)	**Membership function of grid cell (Values >1 include weightings)**
Valley elevation	
$138.42 < Y \leq 155.09$	1
$91.18 \leq Y \leq 138.42$	$0.5 \times (1 - COS(\pi \times (Y - 91.18) / (138.42 - 91.18)))$
$155.09 < Y \leq 202.32$	$0.5 \times (1 + COS(\pi \times (Y - 155.09) / (202.32 - 155.09)))$
$Y < 91.18$ or $Y > 202.32$	0
Elevation	
$168.78 < Y \leq 193.00$	1
$60.00 \leq Y \leq 168.78$	$0.5 \times (1 - COS(\pi \times (Y - 60) / (168.78 - 60)))$
$193.00 < Y \leq 440.19$	$0.5 \times (1 + COS(\pi \times (Y - 193) / (440.19 - 193)))$
$Y < 60.00$ and $Y > 440.19$	0
Major terrain percent upslope	
$35.51 < Y \leq 42.85$	1
$25.05 \leq Y \leq 35.51$	$0.5 \times (1 - COS(\pi \times (Y - 25.05) / (35.51 - 25.05)))$
$42.85 < Y < 52.95$	$0.5 \times (1 + COS(\pi \times (Y - 42.85) / (52.95 - 42.85)))$
$Y < 25.05$ or $Y > 52.95$	0
Hazard site	
Y = Within polygon	1
Y = Outside polygon	0

Table 9. *Fuzzy logic models developed for Sand Hill.*

Dependent variable	**Model**	**Max score possible**
Golden eagle telemetry	Distance to major valley + 2×Percent up slope + 2× Percent up major terrain slope + Gross slope + 2×Subwatershed orientation + 3×Ridge orientation + 10×Hazard site	29
Golden eagle flights	Ridge orientation + Subwatershed orientation + 2×Percent up slope + 0.75×Hill size	7.75
Golden eagle fatalities	3×Hazard site + (Ridge elevation + Major valley elevation)×RidgeValley + Slope to gross slope×RidgeValley	6
Golden eagle combined	(Telemetry positions/29 + Flights/7.75 + Fatalities/6)/3	1
Red-tailed hawk kiting	2×(Percent up slope + Percent up major terrain slope) + Ridge orientation + 1.5×Subwatershed orientation	10.5
Red-tailed hawk fatalities	3×Hazard site + Elevation + Ridge elevation + Percent up major terrain slope	6
Red-tailed hawk combined	(2× (Red-tailed hawk kiting/10.5) + (Red-tailed hawk fatalities/6))/3	1
American kestrel kiting	3×Hazard site + Subwatershed orientation + Ridge orientation + Percent up slope + Percent up major terrain slope + Hill size + Gross slope	12
Burrowing owl burrows	2.5×Percent up slope + Subwatershed orientation	3.5
Burrowing owl fatalities	2×Hazard site + Elevation + 2×Valley elevation + Percent up major terrain slope	6

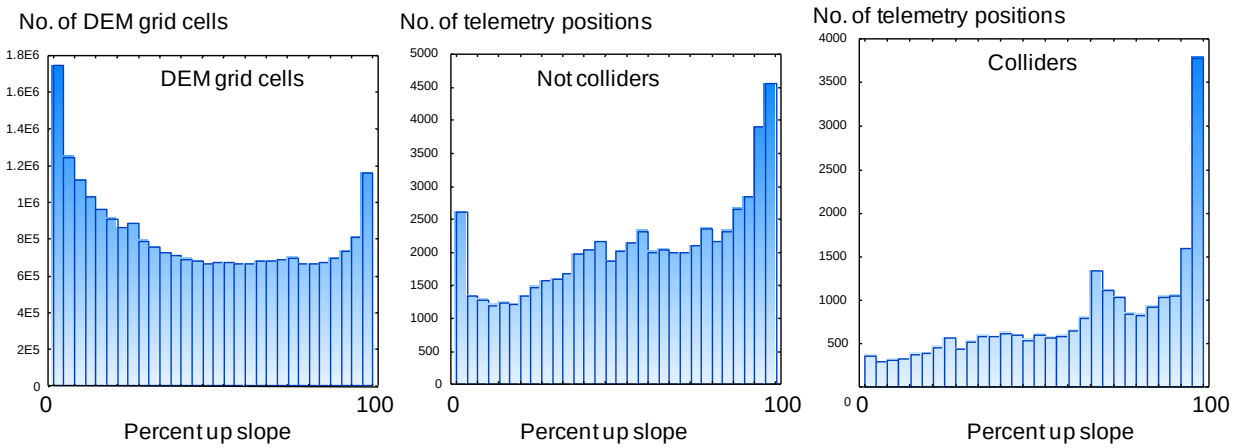

Figure 27. The distributions of telemetered eagle positions were shifted up the slopes (middle and right graphs) compared to the distribution of DEM grid cells in the APWRA (left graph).

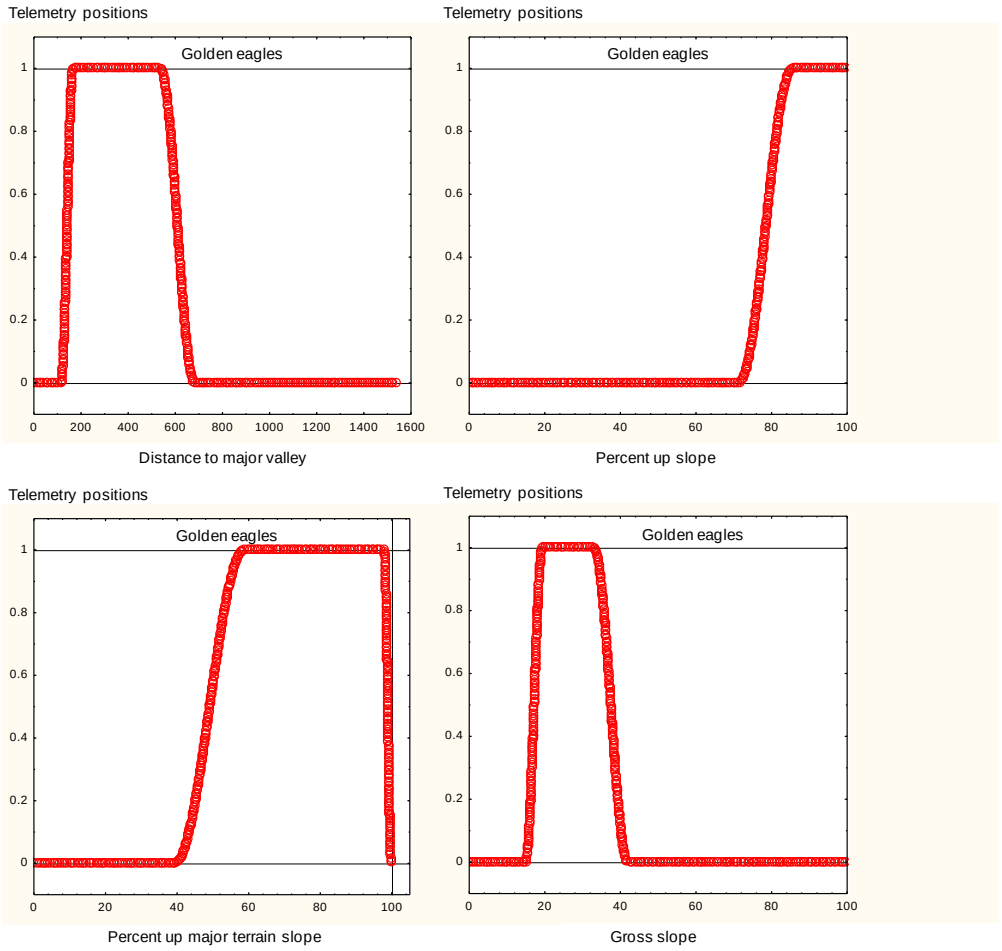

Figure 28. *Examples of grid cell membership values in respective fuzzy logic sets for telemetry positions related to four predictor variables.*

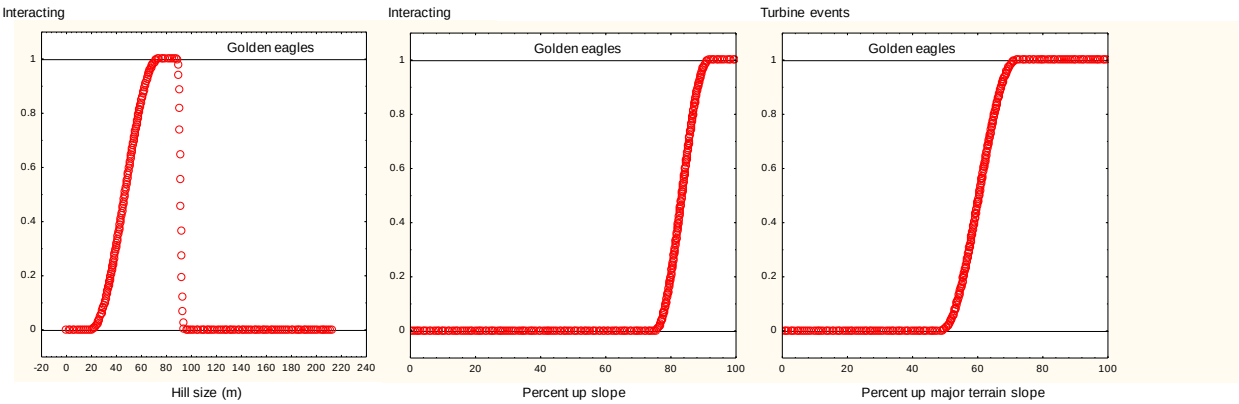

Figure 29. *Examples of grid cell membership values in respective fuzzy logic sets for three predictor variables, including of golden eagle interactions with other birds (left and middle) and wind turbine events (right).*

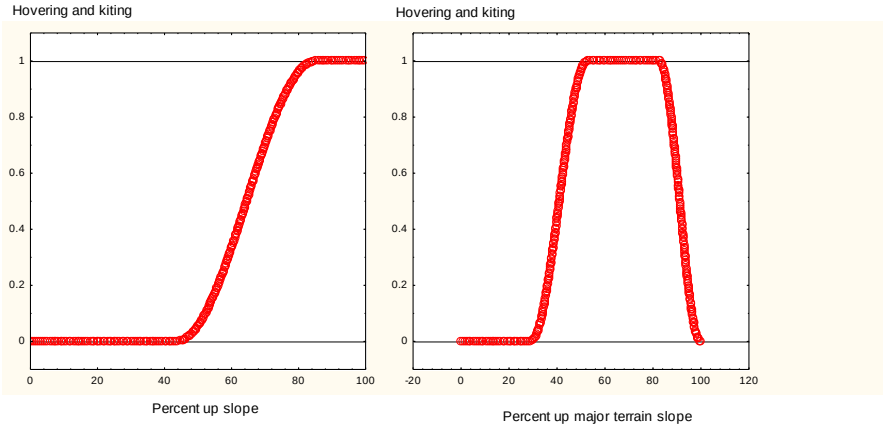

Figure 30. *Examples of grid cell membership values of red-tailed hawk hovering and kiting in respective fuzzy logic sets for percent upslope (left) and percent upslope of major terrain (right).*

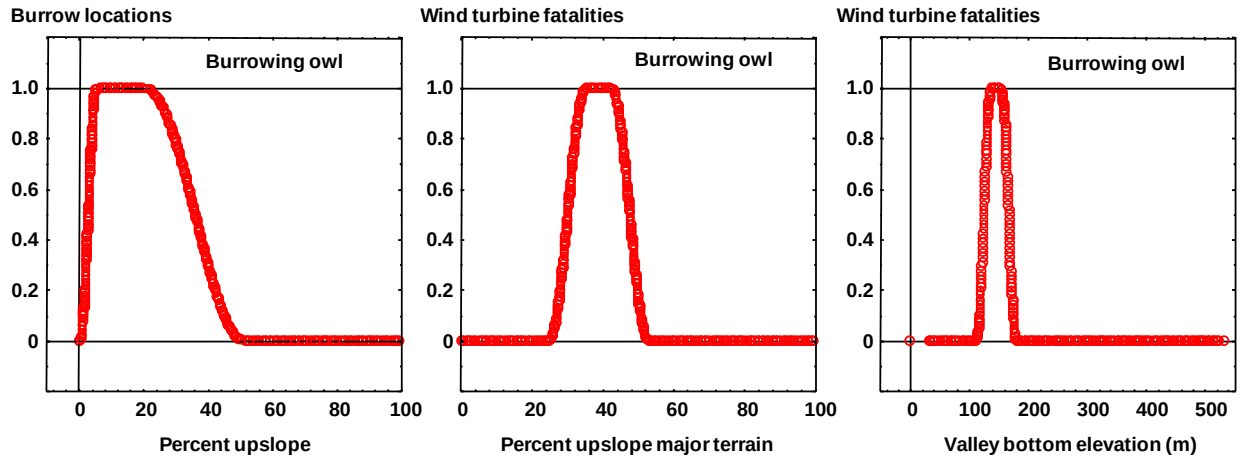

Figure 31. *Examples of grid cell membership values in respective fuzzy logic sets for three predictor variables, including of burrowing owl burrow locations (left) and burrowing owl fatalities at wind turbines (middle and right) in the study area.*

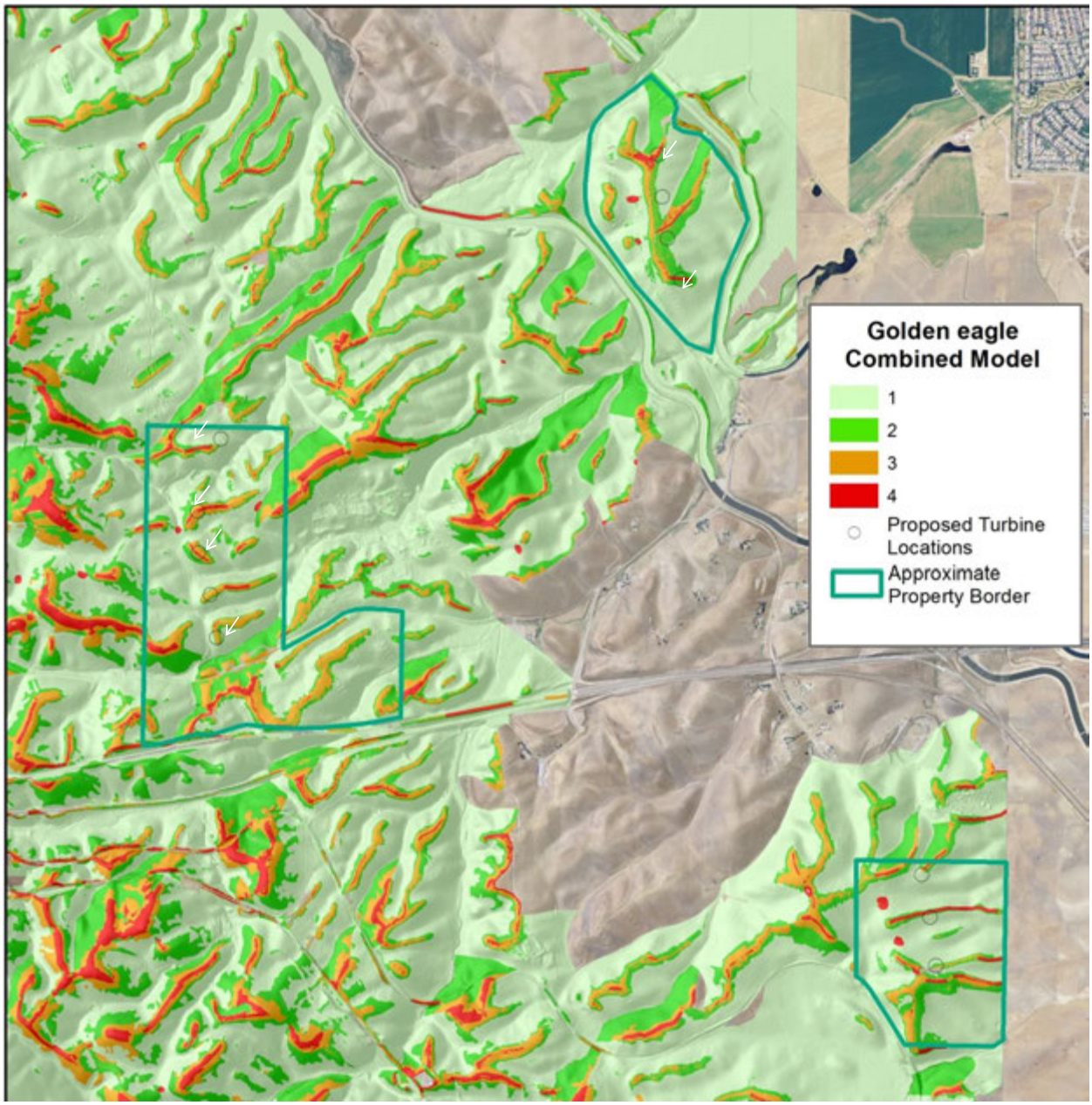

Figure 32. *Fuzzy Logic likelihood surface classes of golden eagle ridge crossing and fatality locations across the Sand Hill project area, Altamont Pass Wind Resources Area, California, where red corresponds with the highest likelihood of golden eagle collision, orange corresponds with the second highest likelihood, dark green corresponds with the third highest likelihood, and light green corresponds with the least likelihood. White arrows point to where we recommended Ogin relocates wind turbines from originally planned sites (open circles).*

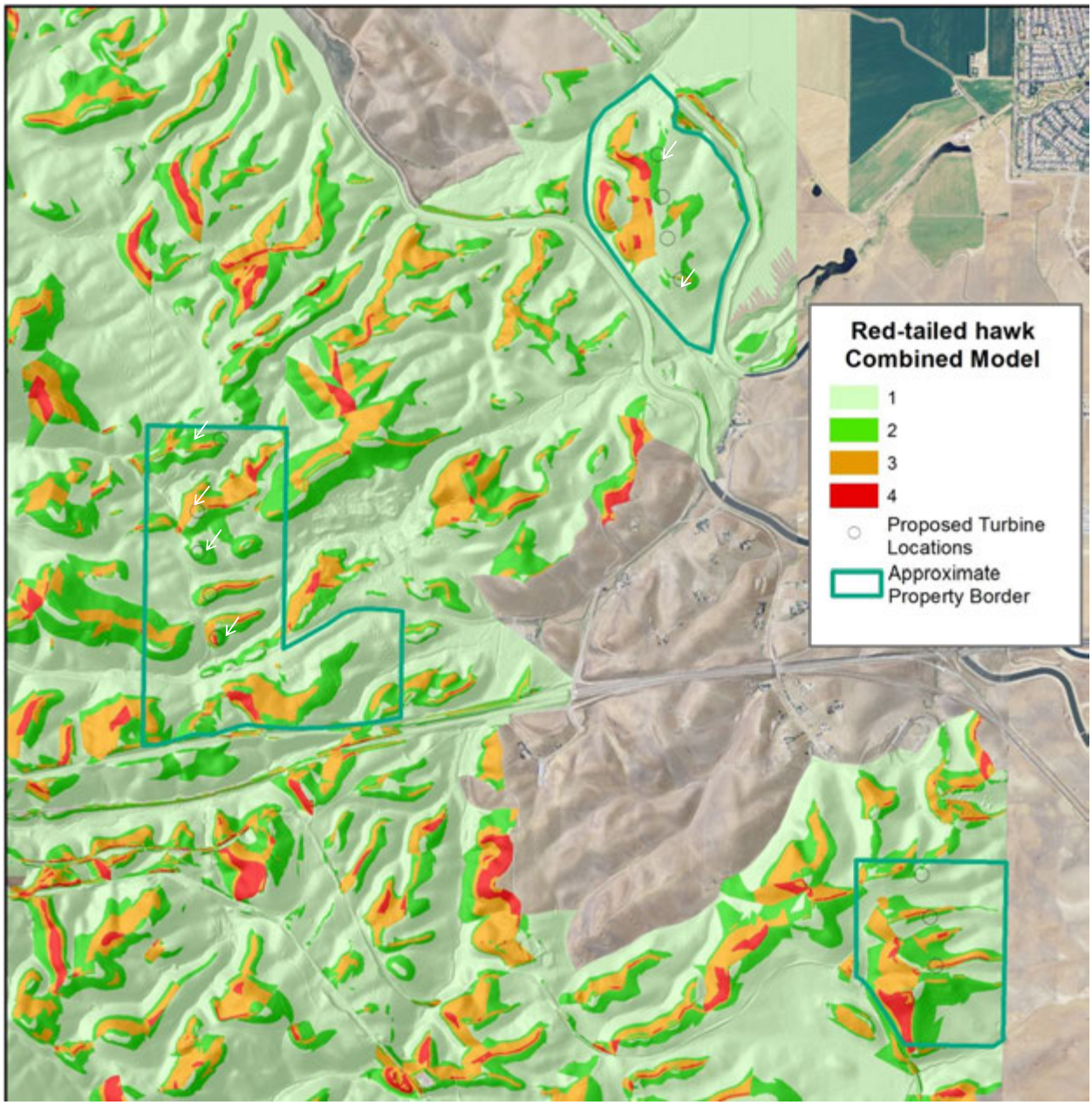

Figure 33. *Fuzzy Logic likelihood surface classes of red-tailed hawk kiting and hovering locations across the Sand Hill project area, Altamont Pass Wind Resources Area, California, where red corresponds with the highest likelihood of red-tailed hawk collision, orange corresponds with the second highest likelihood, dark green corresponds with the third highest likelihood, and light green corresponds with the least likelihood. White arrows point to where we recommended Ogin relocates wind turbines from originally planned sites (open circles).*

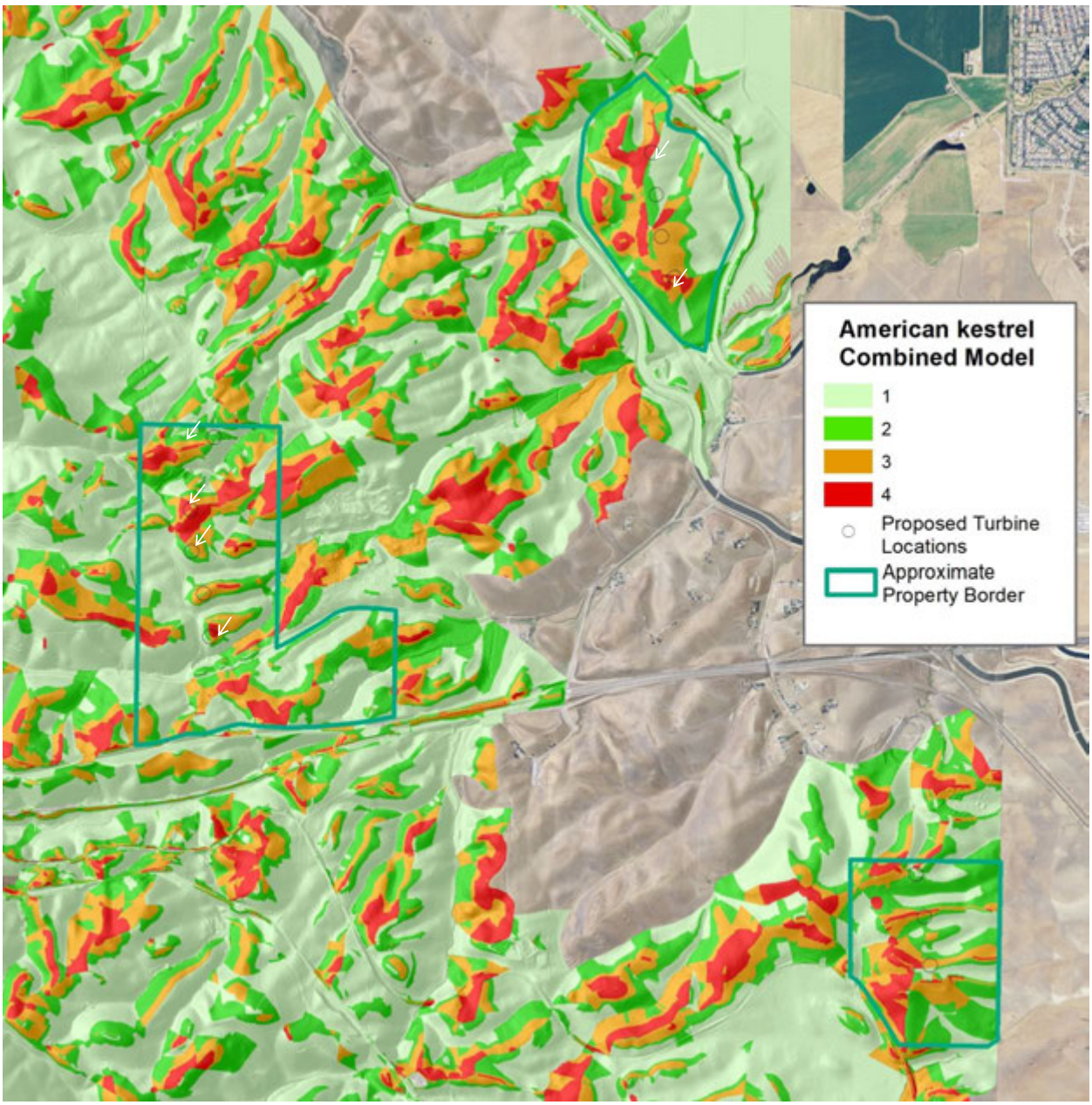

Figure 34. *Fuzzy Logic likelihood surface classes of American kestrel kiting and hovering locations across the Sand Hill project area, Altamont Pass Wind Resources Area, California, where red corresponds with the highest likelihood of American kestrel collision, orange corresponds with the second highest likelihood, dark green corresponds with the third highest likelihood, and light green corresponds with the least likelihood. White arrows point to where we recommended Ogin relocates wind turbines from originally planned sites (open circles).*

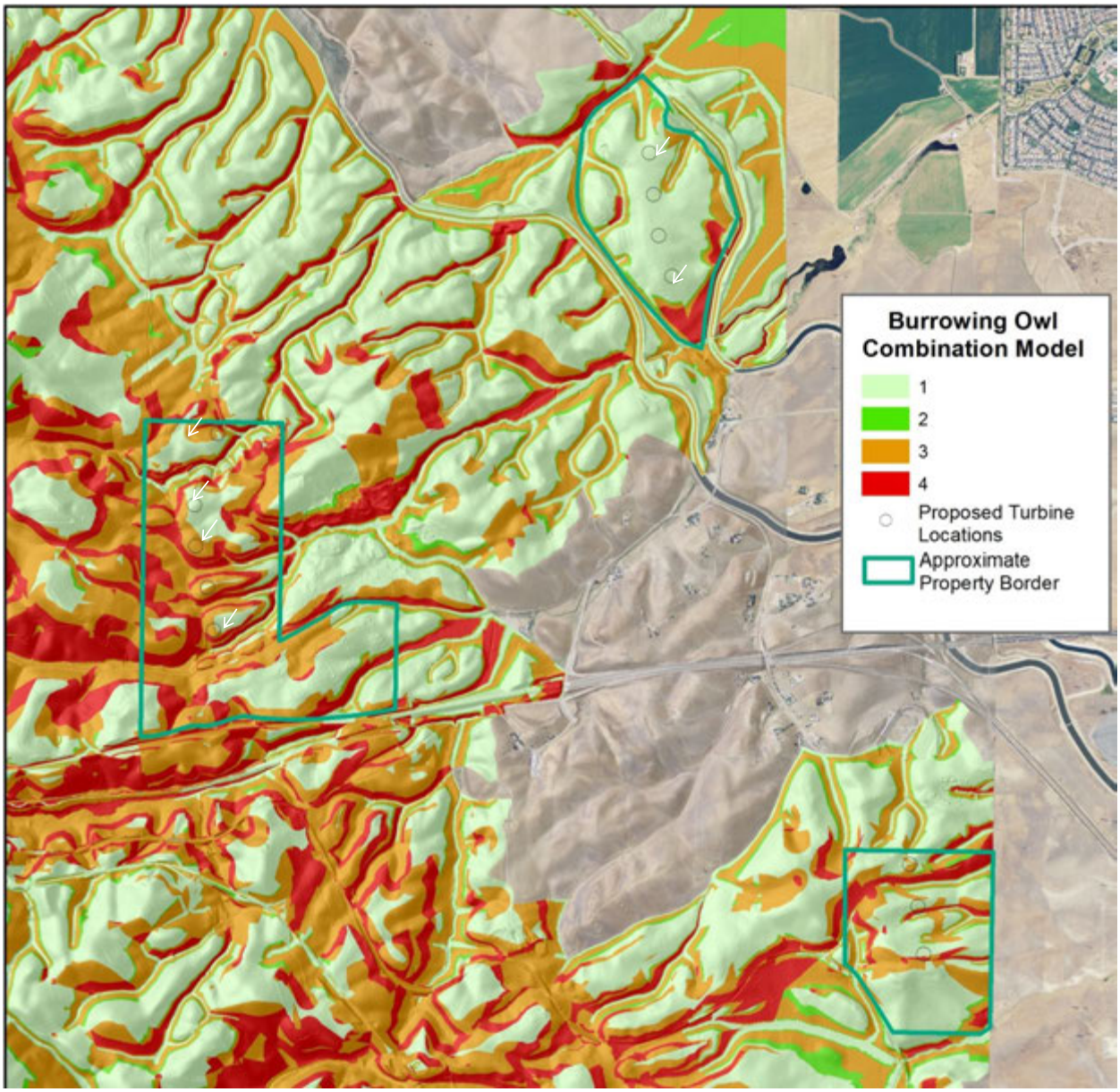

Figure 35. *Fuzzy Logic likelihood surface classes of Burrowing owl burrow and fatality locations across the Sand Hill project area, Altamont Pass Wind Resources Area, California, where red corresponds with the highest likelihood of burrowing owl collision, orange corresponds with the second highest likelihood, dark green corresponds with the third highest likelihood, and light green corresponds with the least likelihood. White arrows point to where we recommended Ogin relocates wind turbines from originally planned sites (open circles).*

DISCUSSION

We produced simple map-based collision hazard models of golden eagle telemetry positions, ridge crossing flights, wind turbine events, and wind turbine fatalities, as well as of red-tailed hawk fatalities and red-tailed hawk and American kestrel hovering and kiting flights in the Altamont Pass Wind Resource Area. We also produced simple collision hazard models of burrowing owls based on burrow locations and fatalities at wind turbines. We extended these models to the Sand Hill project area, which included areas where flight behavior data and burrowing owl burrow data were collected for developing the collision hazard models. After three years of operations at Vasco Winds, and compared to the old-generation wind project that preceded it, Brown et al. (2015) estimated fatality rate reductions of 75% to 82% for golden eagle, 34% to 47% for red-tailed hawk, and 48% to 57% for American kestrel, and 45% to 59% for burrowing owl.

The collision hazard models developed for Sand Hill should perform better than those implemented at Vasco Winds. The golden eagle model was based on a larger behavior data set, GPS/GSM telemetry positions, and fatality rates. The golden eagle model should be more robust than the simple model of golden eagle flights that was developed for Vasco Winds. Our collision hazard models should also be much improved over the models developed at Vasco Winds for red-tailed hawk, American kestrel and burrowing owl.

The collision hazard models likely include some scattered small areas of surface class 4 where it should not have been predicted. Collision hazard models based on millions of analytical grid cells will always include such scatterings of anomalous results, which is why they need to be regarded as guidance tools rather than hard boundaries. Map-based collision hazard maps need to be interpreted carefully, meaning the hazards of specific terrain and wind situations – ridge saddles, apices of southwest and northwest-facing concave slopes, and breaks in slope – should always trump model predictions.

As an example of the need for interpreting hazard maps, our collision hazard models do not account for grading that will be necessary for access roads and wind turbine pads. Changes in the shape of the hills due to grading can transform the location to a more hazardous situation than was assessed herein.

Whereas we focused on four target raptor species, Sand Hill could have adverse impacts on bats and small birds. We developed no collision hazard maps for bats or small birds. We predict that small bird fatalities will lessen as a result of the repowering project, because the project will result in fewer hazardous obstacles on the landscape and airspace will open up for small birds during migration and resident activities. As for bats, we have no way of predicting the project's impacts because we lack sufficient on-site data on fatality rates at old turbines and activity patterns. Whereas we have data on activity patterns of bats at Sand Hill, we lack enough data to predict risk or where the risk might be greatest.

Probably the largest adverse impact to wildlife caused by Sand Hill has been the collision fatalities of burrowing owls. Many burrowing owls nest in the Sand Hill area, and many collided with the old-generation wind turbines. During nocturnal surveys using a thermal camera,

Smallwood observed many near misses between burrowing owls and wind turbines, as well as one collision of a burrowing owl with the nacelle of a broken turbine. Burrowing owls hover and kite in high winds after dark, often doing so upwind of, below, or just behind operating turbine rotors. With fewer operating rotors on the landscape, and with more of the rotor plane occurring much higher off the ground, the repowered wind project at Sand Hill should reduce burrowing owl fatalities by 90% or more.

Table 9. *Micro-siting recommendations directed to Sand Hill wind turbine layout 3 and actions taken by Ogin, Inc. Implications for target species prior to recommended turbine relocations (left columns) and after Ogin's decisions whether relocations were feasible (right columns), where GOEA = golden eagle, RTHA = red-tailed hawk, AMKE = American kestrel, and BUOW = burrowing owl. Shifting turbine relocations according to our recommendations will make no difference to collision risk of American kestrels and burrowing owls, but it will reduce risk by two-thirds for golden eagle and by half for red-tailed hawk. Whereas predicted hazard classes 3 and 4 composed only 16.5% of the landscape for golden eagle, red-tailed hawk and American kestrel (a bit more for burrowing owl), the final turbine layouts will result in only 2 (16.7%) of the turbines within class 3 or 4 hazard zones for golden eagle and red-tailed hawk, 7 (58.3%) of the turbines in hazard class 3 or 4 hazard zones for American kesrel, and 4 (33.3%) of the turbines within hazard classes 3 or 4 for burrowing owl.*

	Overlaps hazard class 3 or 4						Overlaps hazard class 3 or 4			
Site	GOEA	RTHA	AMKE	BUOW	Suggested move	Could Ogin accommodate?	GOEA	RTHA	AMKE	BUOW
1R	Near	No	No	Yes	Move west to site 1A	Yes	No	No	No	Yes
2R	Yes	No	Yes	No	Move 30 m north	Yes	No	Yes	Yes	No
3R	Yes	No	Yes	Yes	Move 30 m NE	Yes	No	No	Yes	Yes
4R	Yes	Yes	Near	Near	None	---	Yes	No	Near	Near
5R	Yes	Yes	Yes	Yes	Move 35 m ENE	No	No	No	Yes	Yes
6R	Yes	No	Yes	No	Move 30 m ESE	Yes	Yes	No	Yes	No
7R	No	No	No	No	None	---	No	No	No	No
8R	No	No	Yes	No	None	---	No	No	Yes	No
9R	Yes	Yes	Yes	No	Move 30 m S	Yes	No	No	Yes	No
10R	Near	No	No	Yes	None	---	Near	No	No	Yes
11R	Near	No	Near	Near	None	---	Near	No	Near	Near
12R	Near	Yes	Yes	Near	None	---	Near	Yes	Yes	Near
Yes:	6	4	7	4			2	2	7	4

ACKOWLEDGEMENTS

We thank Ogin, Inc. for the opportunity to develop map-based guidelines for raptor-safe wind turbine siting. We also thank East Bay Regional Park District, California Energy Commission's Public Interest Energy Research program, NextEra Renewables, and EDF Renewables for earlier funding of research that prepared us for this project. Directed behavior surveys were performed since 2012 by K. S. Smallwood, H. Wilson, E. Walther, B. Karas, J. Mount, S. Standish, and E. Leyvas. We thank D. Funderburg, S. Michehl, Leah Neher, and S. Neher for digitizing bird locations from hard-copy maps. We thank D. Bell for use of GPS/GSM telemetry data of golden eagles.

REFERENCES CITED

Bell, D. A. and C. Nowell. 2015. GPS Satellite Tracking of Golden Eagles (Aquila chrysaetos) in the Altamont Pass Wind Resource Area (APWRA) and the Diablo Range. Main Report-Active Birds For the Quarters ending in March and June 2015. Report to Parties to Repowering Agreement with California Attorney General, Oakland, California.

Brown, K., K. S. Smallwood, J. Szewczak, and B. Karas. 2015. Final 2012-2015 Annual Report Avian and Bat Monitoring Project Vasco Winds, LLC. Prepared for NextEra Energy Resources, Livermore, California.

Brown, K., K. S. Smallwood, J. Szewczak, and B. Karas. 2014. Final 2013-2014 Annual Report Avian and Bat Monitoring Project Vasco Winds, LLC. Prepared for NextEra Energy Resources, Livermore, California.

Brown, K., K. S. Smallwood, and B. Karas. 2013. Final 2012-2013 Annual Report Avian and Bat Monitoring Project Vasco Winds, LLC. Prepared for NextEra Energy Resources, Livermore, California. http://www.altamontsrc.org/alt_doc/p274_ventus_vasco_winds_2012_13_avian_bat_monitoring_report_year_1.pdf

Smallwood, S. 2012. Status of avian utilization data collected in the Altamont Pass Wind Resource Area, 2005-2011. http://www.altamontsrc.org/alt_doc/p231_smallwood_apwra_use_data_2005_2011.pdf

Smallwood, K. S. 2013. Comparing bird and bat fatality-rate estimates among North American wind-energy projects. Wildlife Society Bulletin 37: 19-33.

Smallwood, K. S. and C. Thelander. 2004. Developing methods to reduce bird mortality in the Altamont Pass Wind Resource Area. Final Report to the California Energy Commission, Public Interest Energy Research – Environmental Area, Contract No. 500-01-019. Sacramento, California. 531 pp.

Smallwood, K. S. and B. Karas. 2009. Avian and Bat Fatality Rates at Old-Generation and Repowered Wind Turbines in California. Journal of Wildlife Management 73:1062-1071.

Smallwood, K. S. and L. Neher. 2010a. Siting Repowered Wind Turbines to Minimize Raptor Collisions at the Tres Vaqueros Wind Project, Contra Costa County, California. Draft Report to the East Bay Regional Park District, Oakland, California.

Smallwood, K. S. and L. Neher. 2010b. Siting Repowered Wind Turbines to Minimize Raptor Collisions at Vasco Winds. Unpublished report to NextEra Energy Resources, LLC, Livermore, California. 32 pp.

Smallwood, K. S., L. Neher, and D. A. Bell. 2009a. Map-based repowering and reorganization of a wind resource area to minimize burrowing owl and other bird fatalities. Energies 2009(2):915-943. http://www.mdpi.com/1996-1073/2/4/915

Smallwood, K. S., L. Rugge, and M. L. Morrison. 2009b. Influence of Behavior on Bird Mortality in Wind Energy Developments: The Altamont Pass Wind Resource Area, California. Journal of Wildlife Management 73:1082-1098.

Smallwood, K. S., L. Neher, D. Bell, J. DiDonato, B. Karas, S. Snyder, and S. Lopez. 2009c. Range Management Practices to Reduce Wind Turbine Impacts on Burrowing Owls and Other Raptors in the Altamont Pass Wind Resource Area, California. Final Report to the California Energy Commission, Public Interest Energy Research – Environmental Area, Contract No. CEC-500-2008-080. Sacramento, California. 183 pp. http://www.energy.ca.gov/2008publications/CEC-500-2008-080/CEC-500-2008-080.PDF

Tanaka, K. 1997. An Introduction to Fuzzy Logic for Practical Applications. Springer-Verlag, New York.